A STUDY OF EXCITED LEVELS IN Be^8 VIA THE REACTION $Li^6(He^3, p)Be^{8*}$

Thesis by

Fernando B. Morinigo

In Partial Fulfillment of the Requirements

for the Degree of

Doctor of Philosophy

California Institute of Technology

Pasadena, California

1963

DEDICATION

To the memory of Ernst Ophuls,

"Ernie"

whose short courageous life shall be a perpetual

source of inspiration to those who knew him.

TABLE OF CONTENTS

TABLE OF CONTENTS (continued)

TABLE OF CONTENTS (continued)

ABSTRACT

The excited levels of Be^8 in the region of excitation energies between 14 MeV and 17 MeV have been studied by observing the spectrum of protons produced in the reaction $Li^6(He^3,p)Be^{8*}$. Detailed spectrum studies were carried out with a magnetic spectrometer at bombarding energies between 1.6 and 2.8 MeV at 90° in the laboratory. The structure observed consisted of two peaks in the proton spectrum, corresponding to excitation energies of 16.631 ± 0.006 and 16.941 ± 0.008 MeV in Be^8. No trace of any other level was found at the excitation energies studied. A narrow level near 16.08 MeV would have been observed if the production cross section had been larger than 0.1 millibarns per steradian. The widths in the center of mass system for the two observed peaks have been determined to be 82 ± 6 and 93 ± 7 keV.

Both of these levels were found to decay into alpha particles. The spectrum of alpha particles showed a plateau-like structure corresponding to the breakup of these levels. The detailed shape of the structure is deducible from a kinematic analysis involving energy and momentum conservation, and the observed angular distribution of the outcoming protons.

The angular distribution of the protons leading to these levels has been measured at bombarding energies of 2.2, 2.4, and 2.6 MeV.

Cross sections were measured at angles between 0 and 150 degrees in the laboratory. The angular distributions of the protons leading to the lower level at 16.63 MeV all show a single forward peak; that for the 16.94 level was not observed with sufficient accuracy to show an unambiguous pattern; there is a suggestion of a dip at forward angles with a maximum near 40 degrees.

These angular distributions may be interpreted in terms of a direct mechanism involving the transfer of a neutron and a proton as a single lump. The analysis suggests that the 16.63 level is probably produced by capturing the deuteron into an orbit of zero angular momentum about the Li^6 as a core; the angular distribution of the protons leading to the higher level is compatible with an assumed capture into an orbit of $L = 2$, but the evidence is generally weaker, so that other possibilities are not strongly ruled out.

The interpretation of the data has been carried out using a plane-wave theory of stripping. A brief consideration is given to possible effects of distortions of the plane-wave motion, and the possible effects of the electrical polarizability of the bombarding particles.

An explanation of the angular distributions and the magnitudes of the cross sections is offered; it is suggested that these measurements tend to confirm the guess that the level at 16.63 is the $T = 1$ analog of the $J = 2^+$ ground states of Li^8 and B^8. The level at 16.94 should then be $T = 0$. If one optimistically disregards the weakness of the evidence, the assumed capture into an $L = 2$ orbit suggests that it may have $J = 4^+$.

ACKNOWLEDGEMENTS

The studies that make up the matter of this thesis would never have been finished without the patient teaching and constant encouragement of the many members of the staff of the Kellogg Radiation Laboratory. The author is deeply indebted to Professor Charles A. Barnes, his director of research, for several years of guidance, supervision, and criticism in these and many other studies. He also wishes to express his thankfulness toward Professor Thomas Lauritsen for supervision and criticism in the preparation of the thesis.

The author is particularly grateful to Dr. Emery Nordberg, whose own research served for an apprenticeship, and who aided in the taking of data for the early runs, and to Mr. Ivo Tammaru, who spent a good part of a summer taking data and patching up the equipment so that the bulk of the later runs could be completed in a reasonable time.

The theoretical section has profited from discussions with Professor Robert F. Christy, who supplied valuable leads and comments, from discussions with Dr. H. C. Newns of the University of Liverpool, and from a critical reading by Dr. William G. Wagner.

Finally, the author would like to express his appreciation for financial support from the California Institute of Technology, in the form of tuition scholarships and graduate assistantships from 1957 to 1962.

This work was supported in part by the joint program of the Office of Naval Research and the U. S. Atomic Energy Commision.

I. INTRODUCTION

1. The Energy Levels of Be^8

The study of the production of the levels of Be^8 and of their subsequent decays has proved unusually useful in elucidating many aspects of the physics of nuclei, principally because the nucleus Be^8, in its excited levels of even spin and parity, breaks up promptly into two alpha particles, which are easily detectable in the laboratory and thus yield information about the recoiling nuclear state. The lowest states of Be^8 have a spin sequence 0^+, 2^+, 4^+, as is shown in Figure 1, with the higher of these levels having very large widths because the decay into two alpha particles is very prompt. This sequence makes up a rotational band in Be^8; an unsophisticated description might say that these levels correspond to states of two alpha particles rotating about each other. Beginning at an excitation somewhat above 16 MeV, Be^8 shows some levels which are much too narrow to be explainable with such a crude model. This narrowness must be explained in terms of some selection rule inhibiting the decays. For states which can break up into two alpha particles, we may attempt to explain the small widths in terms of an isotopic spin selection rule, since two alpha particles evidently correspond to a $T = 0$ wavefunction, and at these excitation energies one expects some $T = 1$ levels

corresponding to the ground state and first few excited states of Li^8 and B^8. However, the known levels of Li^8 and B^8 are too few to explain all the narrow levels seen in this region as being of isotopic spin T = 1. In particular, only one of the levels at 16.63 and 16.94 MeV may correspond to the ground state of Li^8 or B^8. The usual procedure of subtracting Coulomb energies is not in this case sufficiently accurate to lead to an unambiguous assignment of a correspondence. The identification of the proper T = 1 level is of some significance in connection with the interpretation of the results of measurements of the beta-alpha angular correlations following the decays of Li^8 and B^8 (Nordberg 62).

Of the reactions available to produce these levels, the $Li^6(He^3,p)$ reaction has the advantage of producing protons, which are easily detectable charged particles of relatively long range in absorbers; this may be of great usefulness in considering coincidence studies of the decay modes of the levels involved. With this reaction, the region of interest is easily within range of the accelerator available at the time the experiment was begun, which has a maximum practicable operating voltage near 3 MeV. The (He^3,p) reaction has the further possible advantage of being useful below the threshold for production of neutrons; this would have helped to carry out coincidence studies of the gamma decays under conditions of somewhat lower background than if deuteron-induced reactions had been used. It was also suspected

that the angular distributions might show the characteristics of a stripping process, since the intermediate nucleus B^9 apparently does not have any sharp levels at these bombarding energies (Ajzenberg-Selove 59). In this case, one might hope that the analysis of the data might be facilitated by the often recurring circumstance that for reactions of very small Q value, the simple plane wave theory of direct reactions gives unambiguous assignments for the value of the orbital angular momentum of the captured particle in its final state (Wilkinson 58).

Three significant previous studies of these levels of Be^8 have been reported. Slattery et al. (Slattery 57), in a study of the Li^7 (d,n) reaction, reported a single level at 16.65 MeV. A somewhat smaller peak corresponding to a level at 300 keV higher excitation was also observed at this time, but it was attributed to an oxygen contamination. In hindsight, it seems quite likely that this smaller peak may have been a structure at least in part due to the level at 16.94 MeV. Dietrich and Cranberg have published a brief report of a study of the angular distributions of the neutrons from this reaction; arguing from the analogy of the angular distributions of the neutrons to the angular distributions of the protons in the mirror reaction $Li^7(d,p)Li^8$, they assigned a spectroscopic classification $J = 2^+$, $T = 1$ to the level at 16.63 MeV (Dietrich 60). More recently, improved measurements of the Q values and widths have been carried out by Erskine and

Browne (Erskine 61). The chief concern of these authors was with the violation of isotopic spin selection rules; their measurements failed to turn up any qualitative difference between these two levels when populated by the reactions $Li^6(He^3, p)$ or $B^{10}(d, \alpha)$. Their measurements were made at a few angles, with an accuracy sufficient to allow a check on the correct angular kinematic energy dependence corresponding to a residual nucleus of mass 8, but were not comprehensive enough to attempt an identification of a direct reaction mechanism.

The original hope in attempting this experiment was that it might yield information leading to an assignment of spectroscopic classification to these levels, and that it might serve as a necessary preliminary experiment for a later investigation of the gamma decay probabilities. The measurements obtained suggest that there is a considerable difference in the wavefunctions of these two levels when viewed as a clustering Li^6 plus a deuteron. The 16.63 level appears to have the deuteron in an $L = 0$ orbit, and the 16.94 level seems to have it in an $L = 2$ orbit, if the data are interpreted by means of a plane-wave theory.

It is quite unusual that the simple plane-wave theory should give adequate fits in a (He^3, p) reaction. For this reason, until trustworthy distorted-wave calculations are made, or at any rate, better theories of direct interactions are used, the assignments may be cast in doubt. Nevertheless the fact that distinctly different patterns are observed tends to indicate that these two levels have very different

wavefunctions and almost certainly must be of different spin. The additional spectroscopic information that these measurements bring are rather meager, since the allowed spin and parity values are already restricted quite severely by the fact that both levels are known to decay into alpha particles.

2. The Measurements and the Data

The data obtained fall into four distinct groups. A discussion in chronological order may clarify the motivation for the attempted measurements.

The first few runs served to identify and locate the particle groups. A plot of the raw data as obtained with the spectrometer for one such run is shown in Figure 2. Here we see the bumps corresponding to the 16.63 and 16.94 levels, and evidence of a small bump possibly corresponding to the level at 17.64 MeV. There is no visible trace of a bump corresponding to a narrow level at 16.08 MeV. At fluxmeter settings higher than 0.75, the proton spectrum is obscured by a step of protons elastically scattered from the thick target backing. A total of seventeen such detailed spectra were obtained; these are the chief source for the values to be quoted for the Q values and level widths.

The differential cross sections obtained during the first series of runs showed marked asymmetries about 90° in the center of mass system. One such set of points is shown in Figure 10. A measurement

of the angular distribution of the protons therefore promised to be of some interest. The experimental difficulties encountered in attempting to obtain data at extreme forward angles with sufficient accuracy suggested that it might be of some usefulness to study the alpha-particle spectra, since it was deduced (Appendix A) that the angular distributions of the protons should be reflected in the detailed shape of the spectrum of alpha particles. One of the more detailed of the alpha spectra is shown in Figure 3. The feature of interest is the plateau having edges at alpha energies of 7.2 and 3.1 MeV for the bombarding energy and angle used in obtaining the data shown in this figure.

After these spectrometer studies, the alpha particles in such a plateau were measured in coincidence with protons of the 16.63 peak, to ensure the correspondence of the plateau with the breakup of the levels (Figure 8).

Finally, the differential cross sections for proton production were measured by scanning the proton spectrum in the spectrometer; the data obtained are much in the manner of Figure 2, except that usually fewer points were taken over a narrower energy region, and smaller amounts of charge incident on the target were used.

II. EXPERIMENTAL EQUIPMENT AND PROCEDURES

1. General

The source of bombarding particles was the 3 MeV electrostatic accelerator of the Kellogg Radiation Laboratory. The singly charged He^3 beam was used for the reaction studies, and the proton beam was used for occasional measurements of the target thickness and for calibrations. The incident energy was analyzed electrostatically; the analyzer has been described elsewhere (Fowler 47). Modifications and improvements made in the suspension and regulating systems have been described in detail by Bardin (Bardin 61). The reaction products or the elastically scattered particles were analyzed by the sixteen-inch magnetic spectrometer. This instrument has been described at length by C. W. Li (Li 51); the recent changes in the fluxmeter and other accessory equipment have been described by Bardin (Bardin 61).

The particle detector at the focus of the spectrometer was either a CsI crystal scintillator and photomultiplier arrangement, or a diffused silicon counter. The particle detectors mounted in the target chamber were usually of the gold-on-silicon type and were constructed either by the author or by Dr. A. B. Whitehead, following the general procedures outlined by Nordberg (Nordberg 61).

The targets consisted of a thin layer of Li^6 metal of 99.3 percent purity, evaporated in the target chamber by means of an electrical furnace, either on thick backings of copper or tungsten, or on aluminum foils of various thicknesses. Since target problems were numerous and of different types for the various measurements to be made, their description is deferred to a later section.

The pulses from the solid-state detectors, or from the CsI crystal and photomultiplier in the spectrometer, were usually recorded after conventional amplification by means of decade scalers with integral bias. For some of the runs involving detection of very low energy protons, a 400-channel pulse height discriminator was used to attempt a more reliable separation between real pulses and the noise.

For the coincidence runs, the gating system of the 400-channel pulse height discriminator proved to be of sufficiently short resolving time to make more sophisticated circuitry unnecessary.

The various particle pulses were counted for fixed amounts of charge incident on the target, as measured by a beam current integrator. All of the electronic equipment was turned on or off by appropriate signals from the integrator.

Very soon after the experiment was begun, it became clear that the limiting factors in the eventual accuracy of the measurements contemplated depended on the characteristics of the target and its stability under bombardment, rather than in the stability or reliability of the

analyzer, spectrometer, or electronic equipment. For this reason, the equipment was used in a way that did not take full advantage of the maximum accuracy and reproducibility obtainable with unhurried careful work. The experimental procedures were rather chosen so as to minimize target problems and at the same time achieve an acceptably efficient rate of taking data. These considerations on the maximum useful accuracy explain the occasionally cavalier treatment given to the analyzing and recording equipment.

2. Measurements of Q Values and Level Widths

In order to obtain reasonable counting rates, allowing the scanning of the entire proton spectrum with sufficient statistical accuracy in a matter of hours, target thicknesses of at least 2×10^{18} atoms/cm^2 were required. The maximum beams that were usable were of the order of one microampere; larger beams tended to be unstable and have hot spots which could cause very rapid deterioration of the target. Most of the runs utilized beams of about 0.8 microampere, diffusely focussed, and having a beam spot about three millimeters square.

The corrections to the incident energy due to losses in the target are of the order of tens of kilovolts for He^3 particles at typical bombarding energies near 2 MeV for targets of such thicknesses. Since the Q values are rather low, if the absolute scale of the electrostatic

analysis is known to an accuracy of less than 1 percent uncertainty, it is clear that the largest error may come from the target thickness energy loss correction, since for lithium targets it is difficult to preserve the target thickness within small limits. Surface contaminations or a volume contamination due to slow oxidation turned out to be a much more likely source of error than any other.

The elastic scattering of either protons or the He^3 incoming beam from the thick target backings provided a sufficiently accurate absolute calibration of the equipment (Figure 5). The electrostatic analyzer has been found to keep its absolute calibration well within the limits that might have made frequent recalibrations meaningful in this experiment (Bardin 61). The careful checks were rather aimed at determining the target condition. The target thicknesses were measured at the beginning and end of the runs, at first using a proton beam, and later using the He^3 beam itself to measure the energy loss in the target material. In addition, a crude check on the target condition is continuously provided by the width and position of the observed peaks, which should be consistent with the assumed target thickness, suitably combined with the natural widths of the levels in question, and the instrumental width introduced by the finite resolution of the spectrometer.

The calibration of the angular position of the spectrometer also needs to be known accurately in order to have accurate Q values, particularly in the present case, when the target mass is not much

larger than the projectile mass. However, it was a different angular measurement, that of the target orientation, which was most likely to introduce the largest uncertainties. The energy loss actually measured by scattering off the thick target backings represents the energy loss in traversing the target twice, first going in and then out again; the target thickness can be measured more sensitively by making it effectively thicker through the use of a large angle of incidence, but only if the angle of incidence can be measured accurately. The errors attributable to the measurement of the target orientation turned out to be larger than those attributable to an incorrect calibration of the spectrometer protractor. Because of the much larger energy loss of the He^3 particles compared to the outcoming protons, for the reaction studies it was often advantageous to place the target unsymmetrically, with a small angle of incidence, that is, with the target more nearly perpendicular to the direction of the incident beam. A check on the reliability of the target position measurements was made by scattering protons off the target backings, since the height of the profile step depends sensitively on the angle of incidence. (The formula giving the yield from a thick target appears in Appendix B, as equation B.7). The results suggest that the uncertainty in target orientation was the second largest source of error in the measurements of Q values and level widths.

In the measurements leading to the best values for the excitation energies and level widths the procedure was the following. Before

evaporation of the target, an elastic profile of the thick target backing was taken. The target was then evaporated, and a new profile taken, either with protons or the He^3 beam itself, to provide the initial measurement of the target thickness. Examples of these profiles are shown in Figure 5. The proton spectrum was then scanned, with a resolution in momentum of 115, taking steps of such a size that no narrow peak would be missed. Typical of such spectra is that shown in Figure 2. At the end of the day's run, profiles were again taken on the actual target, and on a blank piece of the target backing which had been shielded during the evaporation, to provide a measurement of the target thickness at the end of the runs, and incidentally further checks on the constancy of the spectrometer calibration.

For these runs, the targets were evaporated on solid blanks of polished copper. At the focus of the spectrometer, the detector was the CsI crystal and photomultiplier arrangement. The noise level was such that integral biasing easily permitted rejection of noise and background to give zero counts when the beam was on the target but the entrance to the magnetic spectrometer was blocked. Aluminum foils of various thicknesses were used in front of the detector in order to range out the elastically scattered singly or doubly charged He^3. This procedure allowed measurements to be made on protons of energies as low as 660 keV. Counting protons at even lower energies was found to be meaningless because of trace amounts of hydrogen in the ion source,

which produced HHH^+ ions accelerated to the nominal machine voltage. Upon striking the target, the ions were split and produced an equivalent small beam of protons at one third the accelerator voltage, which scattered elastically from the target backing, and produced a background of intolerable size for a study of the peaks of interest. The edge of an elastic step due to these protons may be seen at the highest fluxmeter settings shown in Figure 2. At the usual bombarding energies near 2 MeV, the useful range of the spectrometer was for this reason limited to energies of 660 keV or higher, up to the spectrometer limit near 12 MeV.

3. Investigations of the Breakup Spectra

Alpha particles are produced directly in the bombardment of Li^6 by He^3; this populates the broad states of Li^5, which subsequently break up into an alpha particle and a proton. This process undoubtedly accounts for part of the continuous distribution of protons and the continuous distribution of alpha particles observed at all energies allowed by the energy conservation laws. The only prominent feature of the alpha particle spectrum is a plateau-like structure, having its upper edge near 7 or 8 MeV at backward angles, and its lower edge some 3 MeV below that (Figure 3). This structure may be adequately explained as being due to the breakup of the levels of Be^8 at 16.63 and 16.94 MeV excitation. It was of some interest to study the shape of

this structure, since it contains additional information on the breakup mechanism. As will be explained in section (III. 3), the detailed shape of the alpha spectrum plateau is strong corroborating evidence that the overall reaction $Li^6(He^3, p\alpha)\alpha$ proceeds through definite sharp states of Be^8. There is some hope, therefore, in attempting to interpret the proton angular distribution in terms of a direct reaction mechanism involving Be^8 as a free intermediate state, interacting only weakly with the emergent proton.

This alpha plateau was studied in the spectrometer in order to observe the effects of the angular distribution of the protons on the shape of the plateau at a given angle of observation. As will be explained later, the average forward peaking of the proton angular distribution is unmistakably observable in the magnitude of the slope of the top of the plateau (Figure 7).

Some attention was devoted to the structure of the alpha spectrum for another experimental reason. The most efficient manner of measuring the excitation functions for the combined production of the two levels might have been to measure the total production rate of alpha particles in the plateau, which shows up rather easily in the single counter pulse height spectrum for a thin solid state detector placed in the target chamber (Figure 4). The identification of these alpha particles was confirmed by carrying out a coincidence measurement between the alpha particles in this plateau and protons detected in the

magnetic spectrometer, at an energy corresponding to the center of the 16.63 level.

Many attempts were made to carry out these coincidence studies by using two solid state counters in the target chamber itself, and thus increasing the counting rates by having much larger solid angles. However, this turned out to be impracticable because of the extremely low energy of the protons after passing through an absorber thick enough to range out the elastically scattered He^3 beam. An additional difficulty was occasioned by the copious production of very high energy protons leading to the ground state or other low lying excited states in Be^8. These protons were sufficiently energetic to traverse the entire sensitive region of the solid state counters with a very small energy loss, and thus could simulate low energy protons. It was quite clear that some effect such as this must have been involved, because of the extreme sensitivity of the spectral shape to a small change in bias on the semiconductor detector. The deepest silicon detectors then available were thick enough to stop 8 MeV protons in the depleted region; this was a depth insufficient to produce a meaningful spectrum. The lithium-drifted counters were deeper, but were too noisy to allow a measurement of the proton groups of interest at the bombarding energies accessible to the 3 MeV accelerator. The conclusion was that some magnetic filtering was indispensable. Two runs were obtained of alpha particles in coincidence with protons in the spectrometer.

The exceedingly low counting rates would have made a more comprehensive study prohibitively long (Figure 8).

The information obtained turned out to be of some practical interest later, because the plateau of alpha particles allowed a somewhat simpler indirect measurement of target thickness, and was a convenient monitoring device. For this purpose, a relatively thin counter was used, in which protons of 1.5 MeV energy produced the largest proton pulses; this put the entire alpha plateau much higher than the protons in the pulse height spectrum (Figure 4).

4. Angular Distributions of the Protons

The measurement of the proton angular distributions was made by scanning the peaks of the proton spectrum with the magnetic spectrometer, using techniques somewhat cruder but faster than those used in the best determinations of the Q values and the widths. It was assumed that one could afford to allow the target to oxidize without thereby affecting the integrated value of the cross sections under the peaks. It was rather more important to keep the amount of lithium in the target spot nearly constant. Normalization problems were avoided by running complete angular distributions on the same target spot. Frequent checks on the reproducibility of previous points were considered sufficient indication that the targets were adequately stable under bombardment. Because of the finite lifetime of the targets

(they became unsuitable because of contaminations after about fifteen hours of bombardment), the number of points to be taken for each spectrum, and the total amount of charge at each point were reduced, so as to allow a complete angular distribution to be finished in two days' running time.

In order to get data at the extreme forward angles, which are always of great interest in studying direct reactions, the most useful target backings were aluminium foils of 0.8 mils thickness, with a very thin layer of copper evaporated on the aluminium surface before the evaporation of the lithium. At the forward angles, the emergent proton energies were sufficient to go through the aluminium backings without losing very much of their energy and without destroying the angular resolution by multiple scattering; the measurements yielded peaks which were only slightly less well resolved than the thick-backing peaks. For laboratory angles between 45° and 90°, it was possible to use such targets both with a transmission geometry and a reflection geometry, as for the thick backing targets. The only discernible difference in such spectra was a slight broadening in the transmission spectra, which was entirely attributable to the multiple scattering and estimated lack of uniformity in the backing thickness. The earliest limitation on these targets came from the local heating, which tended to crinkle up the foils if the beam accidentally became sharply focussed or if it became larger. It was found necessary to run with currents of less

than one third microampere, that is, one third of the usual thick-backing current. This meant that complete angular distributions on the foil backings, in the same detail as the thick backings, were not attainable.

5. Targets

For the measurements of the Q values and the level widths it was essential that the targets should be stable and of a constant, well known thickness and composition. Thick copper backings were found excellent for laboratory angles larger than 45°. At smaller laboratory angles, they might not have been sufficiently smooth. The high heat conductivity permitted the use of beams larger than those permitted by other possible backings. This meant that sufficient statistical accuracy could be obtained with thinner targets, which required smaller energy loss corrections. Even using the copper backings, there was an upper limit to the maximum beam that could be used. With beam currents in the neighborhood of two micro-amperes, the lithium layer evaporated completely very quickly, so that not even the target thickness measurement was possible; the target had already evaporated by the time the initial profile had been taken. On the other hand, very long runs at about one microampere seemed to cause no objectionable deterioration; at the end of a run of several hours, the yield curves were reproducible within statistics.

There appeared to be a systematic lowering of yield at any particular point of a peak, but the deviations were not statistically significant, and may be explained as being due to a thickening of the target due to oxidation rather than to an evaporation of the target material.

The initial purity of the target seemed to be well controlled by the usual unhurried procedures for evaporation of lithium (Ford 1962). The evaporating boat, made of tantalum strips, was first thoroughly outgassed by heating in a good vacuum for several minutes. Then a small piece of clean separated lithium 6 metal (obtained from the Oak Ridge Laboratories) of 99.3 percent purity was cut under kerosene, rinsed in benzene, and placed in the boat. The exposure of the lithium to air at atmospheric pressure was kept to a minimum. Ideally, evaporation of the target was not attempted until the vacuum in the target chamber had become at least as good as twice the best vacuum attainable in the system, which was close to 15×10^{-7} mm Hg.

A convenient method of controlling the target thickness was found in simply using a limited amount of lithium metal in the evaporating furnace. A piece of lithium of one half of a millimeter cube was not difficult to cut and handle, yet provided just enough lithium to begin the evaporation on the back of the target, to get rid of any surface contaminations, stop the evaporation, turn the target blank to receive the lithium, and finish the evaporation. With little practice,

it was found possible to predict the final thickness of the lithium layer to within 50 percent. An immediate measurement of the target thickness by means of the energy loss of the He^3 ions in traversing the target was thought to provide the most reliable target thickness corrections. The proton thicknesses were also frequently measured in order to obtain the best possible values for the actual number of lithium atoms in the target, by using the atomic stopping cross sections for protons from W. Whaling's graphs (Whaling 58).

For the measurements of the angular distributions, it was desirable to have the backings be as smooth as possible in order to extend the measurements far forward. For this purpose, the commercially available sheet tungsten proved to be better than the copper as a target backing. The reliability of the extreme forward angle measurements and the effects of surface irregularities were tested by measuring the target profile for elastically scattered protons at grazing angles of the beam with the plane of the target. Reproducible profiles of the correct absolute magnitude were obtained for all angles of incidence smaller than 75 degrees. The tungsten was chosen in preference to the copper blanks simply because of smoothness. The grain of the residual abrasive action on the best copper blanks, after etching in ammonia-hydrogen peroxide was observed in a high powered microscope to be of about one half micron (0.0005 mm). No grain of comparable size was visible in the tungsten surface. These characteristics made the thick tungsten backings suitable for measurements at

laboratory angles as small as 30 degrees. At forward angles smaller than 30 degrees, the best solution to target problems was found to be the thick foil backings. Thin carbon foils were first tried, but these were unable to stand He^3 beams of the desired size, of at least one third of a microampere. The foils would warp severely under the action of the beam, and they would break almost at once after the evaporation of the lithium. This was attributed to an energy loss effect, since the foils would stand up quite well under prolonged bombardment with proton beams of the same energy. Thin metallic foils were next tried, with somewhat greater success. However, the situation was still quite precarious. The commercially available nickel, gold, and aluminium foils, and copper foils manufactured by the author, all behaved in a similar manner; they all might have served very well at somewhat higher bombarding energies, where energy losses would have been somewhat reduced. The requirements of beam size meant that for these thin metallic foils it was necessary to operate always at the edge of the zone of reliable operation, and small instabilities in the operation of the ion source were sufficient to break the foils. Nevertheless, some useful data were obtained using an aluminium leaf backing, of a thickness near 0.2 milligrams/cm^2.

Most of the measurements at forward angles were obtained with thick foil backings. The aluminium foils were chosen thick

enough to stop the incident He^3 beam, but as thin as possible otherwise. As a rule of thumb, it was found that twice the nominal range of He^3 ions in aluminium provided a stable backing, one that would not warp immediately for momentary surges of the beam current.

An interesting puzzle arose when these thick foils were first used. There appeared to be an immediate deterioration of the target upon bombardment, such that the peaks would be observed in the first scanning, but the results would not be reproducible; in a second scanning, they would be badly broadened and distorted, and appear at lower energies. In a third scanning, their structure would have disappeared into an amorphous continuum. A slow oxidation of the targets, by cautiously exposing them to a small pressure of air, was tried as a means of stabilising the target. The targets became much stabler, but the procedure entailed an unacceptable loss of resolution, since the stopping cross sections in Li_2O or LiOH are two to four times that for an equivalent amount of lithium in metallic form.

It was guessed that the explanation lay in that the lithium was diffusing into the aluminium backing under the action of the local heating caused by the incident beam. In order to circumvent this diffusion, but also to avoid using thick foils with a high atomic charge Ze, the next few runs were attempted with aluminium foils on which a very thin layer of metallic copper had been evaporated under vacuum. It was hoped that the diffusion of the lithium into copper would be slower

than the diffusion into the aluminium, since the solid copper targets had shown no apparent diffusion problems. The resulting targets were found to be quite stable, and no effects of diffusion were discernible. The peaks were in general as well resolved as with the thick copper or tungsten backings when an equivalent care had been taken in the target evaporation.

III. EXPERIMENTAL RESULTS

1. Calibrations

The initial procedure of each day's run consisted in observing the profile of elastically scattered particles on the target backing material. If one assumes that the energy calibration of the electrostatic analyzer is well known, the calibration of the magnetic spectrometer may be determined from the position of the midpoint of the rise of the profile. A convenient discussion of the formulae is given by J. Overley (Overley 61); a brief summary of the actual procedure for calculations in this experiment is given in Appendix B.

These calibrations were necessary in order to determine the reliability of the energy scale for the Q value, so as to have some idea of the accuracy with which the Q values were being measured. In the earlier runs, the calibrations were carried out at such spectrometer settings as were expected to be near those needed for the scanning of the peaks. However, since the overall limiting accuracy lay in the uncertainties in making the target thickness corrections, the extra precaution did not add to the confidence with which one may quote the result. The later calibrations were made at the bombarding energy to be used in the day's run. A typical profile from a tungsten backing appears in Figure 5.

A table of the spectrometer calibration constants measured at various stages of the experiment is included as Table I. Over a period of several months, the variations of the calibration constants measured at many angles and fluxmeter settings were too small to affect significantly the overall uncertainties in the Q values; the root mean square deviation is less than 1 percent. The reproducibility of the spectrometer calibration constant has been taken to be a fair index of the absolute precision of the experiment.

The cross section as determined from the yield of counts versus spectrometer settings is always proportional to a constant determined by the geometry of the spectrometer, and the capacitor and firing voltage of the beam current integrator. In the formula for the cross section for a thin target (Appendix B, equation B.9), this constant is written as $R/CV\,\Omega$, where R is the resolution, C is the capacitance of the capacitor, and Ω is the effective solid angle which the spectrometer accepts. This constant must in practice be determined experimentally by measuring a known cross section. In our case, the known cross section was considered to be the elastic scattering of the incident particles from the target backing, which was assumed to be entirely due to electrical forces, and to be equal to the nonrelativistic elastic scattering from a point-charge nucleus. The corrections for relativistic effects and for electronic screening effects are negligible compared to other uncertainties. The determination of this constant

serves as a calibration for the absolute magnitude of the cross section.

The measured values of the instrumental constant are listed in Table II, in the form of a comparison to the nominal value which this constant would have if we simply accepted the values for the resolution and solid angle previously used by other workers in this laboratory. We take R = 231 for the 1/4 inch slit at the spectrometer focus, and Ω = 0.0063 steradians (Li 51) (Kavanagh 57). The root mean square deviation of 8 percent is compatible with an error estimate combining quadratically the fractional errors coming from all measurements involved. The largest error is attributable to the imprecision in our knowledge of atomic stopping cross sections. The atomic stopping cross sections for protons in copper are relatively well known, but most of the calibrations were run on the tungsten backings, for which no experimental data are available. The stopping cross sections in tungsten were estimated by extrapolation from the values in tantalum and gold (Appendix B), and corrected for very low values of the parameter E/Z by the use of an empirical curve, as suggested in the article by Whaling (Whaling 60).

2. Measurements of Q Values and Widths

The first few exploratory runs served to locate and identify the peaks observed in the proton spectrum. No peaks were observed in the region of excitation energies in Be^8 between 14 and 17 MeV

except two corresponding to levels at 16.63 and 16.94 MeV. Although the level at 17.64 was probably populated to a measurable extent, it was not possible to make measurements on it because the experimental conditions were such that it was always masked by either the protons of 1/3 the accelerator voltage coming in in the form of HHH^+ ions, or the protons knocked out in the forward direction because of hydrogen contamination in the target. The knockout cross section is so large that a small amount of hydrogen, of the order of 1 percent of the number of atoms in the target, is sufficient to mask completely the protons corresponding to the 17.64 level at forward angles.

In order to have uniformity in the treatment of all the spectra, the observed values of the yield as a function of the spectrometer setting were converted to a Q value spectrum before attempting to deduce Q values or widths. A probability distribution as a function of Q value is obtained as follows. If the number of counts obtained at a spectrometer fluxmeter setting of $\underline{I}$ volts is N(I), the distribution as a function of $\underline{I}$ is

$$W(I) = N(I) / I \qquad \text{(III. 2. 1)}$$

(we omit all constants that appear as a factor). We convert to the variable Q by use of a relation giving Q as a function of $\underline{I}$. The definition of Q value given in the Appendix B reduces to the form

$$Q = A + B/I^2 + C/I \qquad \text{(III. 2. 2)}$$

if we neglect relativistic corrections and make the energy loss corrections for the protons only to first order in $\underline{I}$. The quantities A, B, and C are appropriate constants. The Q value distribution is then

$$W(Q) = W(I) / (dQ/dI) . \qquad \text{(III. 2. 3)}$$

This expression is to be evaluated at a definite value of I; the corresponding value of Q is obtained from equation (III. 2. 2). Such a curve represents the probability that the reaction should result in a Be^8 nucleus at an excitation within a differential interval about Q.

An examination of the shapes of the proton spectra, after they had been converted to Q value spectra, showed that the proton peaks would be fitted excellently by a curve of the Breit-Wigner shape. The values to be quoted for the peak location and peak widths are part of the output of a computer program which fitted curves of the following shape to the Q value spectra:

$$W(Q) = \frac{M G^2}{(Q - A)^2 + G^2} + \frac{M' G'^2}{(Q - B)^2 + G'^2} + C \qquad \text{(III. 2. 4)}$$

The variable is Q, and the other quantities are parameters. The quantities G and G' represent one half of the observed widths at half maximum; the natural widths of the levels have been determined by assuming that the instrumental widths and target-thickness widths combined quadratically with the natural widths to give the observed widths. By instrumental widths we mean principally those due to the

finite angle and energy resolution of the spectrometer. For the transmission geometry, the contribution induced by the root mean square scattering angle of the emergent particles was small, but not negligible. A more specific description of the computer program is to be found in Appendix B.

The curves of the shape (III. 2. 4) with the parameters as determined by the computer program have been plotted for every spectrum, in order to ensure that each fit is reasonable and corresponds to physically meaningful values of the parameters. In Figure 6 we show one such fit, corresponding to a case in which the instrumental widths were small, and many points on the spectrum were obtained, so that one may see most directly the natural shape of the spectrum. This fit is not statistically the most favorable one, on the basis of a goodness of fit test. The point of showing this figure is simply to illustrate the suitability of a function of the chosen algebraic shape to represent a typical spectrum.

The best values for the Q values of the levels and their natural widths have been taken to be the averages of the fitted values, using only spectra measured under good conditions, that is, such that the target thickness and its stability were well known. The results of this average, together with the root mean square deviation and the standard deviation of the mean, are given in Table III. Since there was

no obvious way of choosing a weighting factor for the fitted value for each individual spectrum, the fitted values themselves have not been assigned a probable error. As an absolute error, we quote the standard deviation quadratically combined with the estimated absolute error of the energy scale, and an estimated uncertainty attributable to possible surface contaminations.

3. Identification and Shape of the Breakup Spectra

The spectrum of alpha particles produced upon bombardment of Li^6 by He^3 was measured in detail with the magnetic spectrometer, at 90° and 150° in the laboratory, at bombarding energies of 2.2 and 2.6 MeV. One of these spectra is shown in Figure 3.

By assuming that the reaction proceeds through a well defined sharp state of Be^8, it is possible to predict the shape of this spectrum, if one may make some assumptions about the angular distribution of the protons in the reaction, and of the angular distribution of the subsequent breakup. The derivation of these formulae is given in Appendix A. The assumption that the intermediate nucleus is well defined is in a sense equivalent to saying that there is a strong interaction between the two alpha particles after a breakup into three particles.

The shape of the alpha particle spectrum is sensitive to the angular distribution of the emergent protons. In Figure 7 we have

plotted an alpha particle spectrum as a function of the velocity in the laboratory system. The idealized theoretical spectra also shown in Figure 7 represent the spectra to be expected if we assume that only one infinitely sharp state of Be^8 is produced, which subsequently decays freely in its center of mass system. The calculation of the spectral shape is easily done if the angular distribution of the protons in the center of mass system is considered to be of the form: $1 + a \cos\theta$. The slope of the plateau is quite sensitive to the value of a. We see that a value of a near 0.26 approximately describes the degree of forward peaking to be expected for most of the protons in the two groups.

More sophisticated predictions can be made by allowing the intermediate state to split into two, corresponding to different Q values, and then allowing these to have finite widths, but nothing new is learned by carrying out these lengthier computations, except that the fit is much improved. It is interesting that although plateaux of this general shape have often been seen and are reported in the literature (Jarmie 61), with the correct explanation that they are due to a two-stage breakup, the exploitation of the spectral shape as a means of determining the angular distributions of the first particle has not been done. It would seem that the spectral shapes deduced in the Appendix A are sufficiently simple and easy to use, so as to be useful at least in correlating various measurements, as has been done here. The method may even be

useful in connection with the angular distributions of neutral particles or particles not directly observable because of experimental limitations. The results also suggest that there may be inherent dangers in discussing anomalies in spectrum shapes in terms of final state interactions without a simultaneous discussion of angular distributions. Such anomalies have been discussed for measurements done at one angle by Beckner et al. (Beckner 61).

For the measurements of alpha-proton coincidences, the spectrometer was set to accept the center of the peak corresponding to the level at 16.63 MeV excitation, and a solid state counter thin to protons of more than 1.5 MeV energy was placed in the target chamber to detect alpha particles. An aluminium foil in front of the alpha counter ranged out the elastically scattered beam. The resolution of the counter for alpha particles was estimated from the response to the thorium alpha lines; these at the same time provided a sufficiently accurate calibration of the counter. In Figure 8 we show the pulse height spectrum corresponding to the ungated signals, and the pulse height spectrum gated by the proton pulses from the spectrometer counts, after subtraction of the random counts expected from a resolving time of 1.2 microseconds. The actually measured resolving time was 1.2 microseconds only near the expected peak; it was found to be nearly 20 percent longer for the largest pulses. We have taken these

measurements to be evidence that the entire plateau of alpha particles is due to the breakup of the two levels in Be^8.

4. Angular Distributions of the Protons

The data used in determining the angular distribution of the protons were taken by scanning the proton peaks much as for the Q value measurements. Since this was at best a very time-consuming process, it was found necessary to streamline and speed up the procedure in order to get complete angular distributions within the lifetime of a single target. The simplifications and shortcuts inevitably resulted in individual spectra of poorer quality than that shown in Figure 2. Nevertheless, the streamlined procedure probably represented the best compromise in attempting a measurement of the angular distributions.

The reduction of the observed proton spectra into cross sections was eventually reduced to a purely mechanical process, since a computer program was eventually developed which took the raw data directly in the form recorded in the laboratory and converted them into an output in the form of cross sections, in millibarns per steradian, in the center of mass system. A description of the steps in this program is to be found in the Appendix B.

The cross sections are obtained from the fit of the Q value spectra by multiplying the amplitude parameter times the half width

times the factor $\pi/2$. The statistical errors to be assigned to cross sections calculated in this manner are probably smaller than is reasonable if one simply uses the usual rules of partial derivatives, because the parameters of the levels are not as independent as the mathematics suggests. The relative errors to be quoted are a combination of the statistical errors of the points, of the parameter used in the goodness of fit test, and of a reliability parameter that measured the deviations of an individual spectrum from the overall average in the width and the peak centroid parameters.

We have listed the results of the data reduction program in Table IV. For convenience in the presentation of results, the peaks have been given names, peak A corresponding to the level at 16.63 MeV excitation, and peak B corresponding to the level at 16.94. The subscripts A and B have been freely used to denote quantities corresponding to one or the other of the peaks. The statistical errors of the cross sections lie between 5 and 10 percent. As an example of a spectrum which has been considered a generally poor fit, we show the spectrum that fared the worst in the quality criterion in Figure 9. A good spectrum is represented by Figure 6.

The largest single uncertainty in the values of the cross sections comes from the target thickness. The initial measurement of the target thicknesses was made by observing the energy loss of the incident beam in traversing the target material, as determined from the

midpoint of the rise of the profiles (Figure 5). The number of atoms per square centimeter was obtained by assuming the target to be pure lithium 6, using the atomic stopping cross sections for protons on lithium given by Whaling's graphs (Whaling 58). The purity of the target may be estimated from evidence of contaminations. The fact that a great many of the detailed spectra showed no peaks except those corresponding to a Li^6 target when freshly made serves to put an upper limit on the amount of contamination with elements such as carbon and oxygen. The hydrogen contamination, which was troublesome in that it obscured measurements on the 17.64 level, has been estimated to be of the order of 5 percent by number of atoms in the target that gave the largest knockout proton peak. Further estimates of the initial purity may be made by a comparison of the energy losses in traversing the target before and after exposure to a small pressure of air. The evidence in general points to an uncertainty somewhat smaller than 10 percent in the estimate of the amount of lithium in the target.

Even when using the same target spot for all angles at one bombarding energy, the relative errors include an uncertainty due to the target thickness because the orientation of the target relative to the direction of the incident beam changes as the spectrometer angle is changed. For some of the later runs, especially those in which the target backing was an aluminium foil, the target thickness was estimated

from the yield of alpha particles in a solid state counter placed in the scattering chamber. This procedure allowed one to skip the taking of two profiles, and yielded values that were considered less sensitive to contaminations. These considerations lead to an estimated uncertainty of the order of 8 percent for the relative stability and constancy of the amount of lithium in the target.

When plotted as a function of angle, the cross sections at all energies measured showed some of the features of stripping reactions, that is, strong asymmetries about 90° in the center of mass system, with a forward peak. It was therefore decided to attempt to analyze these results in terms of a direct reaction theory. The angular distributions measured at various bombarding energies are shown in Figures 10, 11, 12, 13, and 14. The smooth curves represent the fits obtained by use of the theory described in the next part.

The total cross sections have been determined by integrating the smooth curves for the theoretical fits; the results of these integrations are shown in Table V. The errors quoted represent a quadratic combination of the errors in the relative measurements with the estimated uncertainties in the absolute calibration.

IV. THEORETICAL ANALYSES

1. Introduction

Once the angular distributions had been obtained, it was desirable to interpret the results in terms of the characteristics of the levels. Theories of stripping of two nucleons presumably applicable to (He^3, p) reactions have been developed, notably by H. C. Newns (Newns 60). The fits obtained using the simplest versions of these theories, for example, using formulae suggested by El Nadi (El Nadi 61) were as good as might be expected in the light of the quality of fits in other (He^3, p) reactions (El Nadi 61).

There were two puzzling things about the fits obtained by use of these formulae. First of all, the radius parameter in the fits needed to be energy-dependent, systematically increasing as the bombarding energy was increased from 1.8 MeV to 2.6 MeV. Also, it was puzzling that these fits should be adequate at the very low bombarding energies used in this experiment, since the derivation of the simplest plane-wave theory of Newns or El Nadi suggests that it should be very sensitive to the phase of the wavefunction of the relative motion at the surface of the target nucleus. The theory was being applied below the Coulomb barrier, and giving adequate fits. These two puzzles

were the stimuli of the development of the theory to be presented.

Historically, a qualitative justification for the applicability of plane-wave stripping theories at bombarding energies below the Coulomb barrier has been made on the basis that the particle to be captured may see a smaller barrier than the composite incident particle as a whole (Landau 57), but this justification has never been made quantitative. For actual calculations using perturbation theory, as is customary, the results ought to come from the wavefunctions used for the initial and final states, which are distorted away from the plane-wave form by Coulomb effects, for example. The Coulomb field has two effects. First, the relative motion in the initial and final channels is distorted. Second, even at bombarding energies such that the plane wave approximation is justified for the relative motion, it is possible that the incident composite particle may be polarized by the electric fields as it approaches the target nucleus. Such a distortion of the wavefunctions has been considered in connection with the elastic scattering of deuterons; it was of interest to find out how the elastic scattering of a particle was affected by its polarizability (Ford 62, Renken 62). The results for deuterons suggest that the effects of electrical polarizability should be small for all reactions. These estimates are discussed in Appendix C. The effects of electrical polarizability are entirely neglected in what follows.

2. Direct Reactions Viewed as Three Body Problems

We would like to develop a simple theory to describe nuclear reaction processes involving the exchange of a single nuclear cluster. Symbolically we represent the exchange as follows:

$$(AB) + C \longrightarrow A + (BC) . \qquad (1)$$

The parentheses enclose two clusters which are considered to be in a bound or metastable state before and after the reaction. Our aim is to interpret experimental results in terms of the quantum numbers of the nuclear clusters A, B, and C, which are assumed to have no internal structure but may be endowed with a spin, and in terms of the characteristics of the bound states (AB) or (BC). All of the reactions known as "direct interactions" may be described in this way as a first approximation. For example, (d,n) reactions may be looked upon as the exchange of a proton between the neutron and the target, the (d,p) reactions correspond to exchange of a neutron, and the (p,p'), (p,n) and other "knockout" reactions would correspond to an exchange of the target core between the incoming and outgoing light particles.

The usual theory of direct interactions, especially as applied to (He^3,p) reactions, describes such processes in terms of a specific phenomenological surface interaction of adjustable strength at the surface of the target cluster C. Using first order perturbation theory and using plane waves for the relative motions of the unbound pairs, the resulting description has had enormous success in describing the qualitative features of a great many nuclear reactions when the bombarding energies are such that the three clusters (ABC) are unlikely to form a metastable nuclear state. Refinements of such a theory so

as to estimate the effects of distortions from the plane-wave form of the relative motion result in formulae giving excellent fits to the angular distributions of the final products, provided that the parameters describing the distorting forces are considered adjustable (Tobocman 61). These fits are so good that one may well ask, why not accept the usual theory as valid?

There are some suggestive aspects in which the usual theory is not very satisfactory. A cursory inspection of the symbolic process (1) shows that the clusters A and C appear symmetrically if one reads the process forwards and then backwards. Thus the assumption of a surface interaction at the cluster C involves an artificial desymmetrization of a type ordinarily considered inelegant in physical theories. There is no a priori reason to assume that the angular distributions should depend on the radius of the nucleus (BC) but not on the radius of the nucleus (AB). Another aspect which is puzzling involves the quantum number of the relative orbital motion in (BC). In attempting fits, it is found that strange mixtures of various L values are needed, strange in the light of what one might estimate by assuming that the shell model of the nucleus provides an essentially correct description of the final nuclear state (BC). A third puzzling aspect of the usual theory, particularly apparent in our case, is that the plane wave theory is often found to give excellent fits to the angular distributions at bombarding energies so low that undistorted plane waves might be expected to

give a completely erroneous answer. This point has been the subject of much debate, but the proposed explanations are not quantitative and do not seem to find general support. This lack of agreement is evident, for example, in a reading of the discussions at the Rutherford Jubilee International Conference (Birks 61). A fourth point is that the refinements of the usual theory all introduce new adjustable parameters which add very little to our knowledge of nuclear states. Each of the four parameters of the optical potentials introduced to represent nuclear distortions causes changes in the predicted angular distributions which are so drastic and of such a character that small adjustments, of the order of 5 percent, almost inevitably yield an acceptable fit. Since the plane-wave theory, with its amplitude parameter and scale parameter (the nuclear radius) is already qualitatively correct, it is no wonder that the continuous deformations induced by varying the optical model parameters eventually yield a good fit. The effect of varying these parameters has been studied by W. R. Gibbs (Gibbs 61). One might be happier of the optical model parameters were independently determinable, but if results do not agree, there is no theoretical way out, since the nature of the averaging process that defines the optical model parameters does not guarantee that it should give the same average values for its parameters in different circumstances (Saxon 61).

Some of the modifications of the usual theory which will be used below are implicit in suggestions that have been made in theoretical

papers dealing with the general formalism of scattering theory. Nevertheless these suggestions, in spite of their possible advantages, have not found their way into the habits of experimenters who would like to give an interpretation of their data. For this reason, it has seemed opportune to present these ideas in a unified fashion. The specific changes in the usual theory are the following:

1. One should give up the postulate that direct reactions occur at the "surface" of the cluster C. This change will in general give even better fits to the angular distributions with plane-wave states, and eliminates an inelegant asymmetry in the description.

2. The calculations should include the effects of the interactions between all three pairs of clusters, (AB), (BC), and (AC). This further removes asymmetries in the description.

The plane-wave theory which results from these changes has several advantages over the traditional description due to Butler (Butler 57). First, it is evidently more "symmetric" and therefore has a certain esthetic advantage. Second, the inclusion of the entire nuclear volume has the effect of making the angular distribution less sensitive to small distortions. Third, all the direct reactions, whether of the stripping type or the knockout type or the inelastic scattering type, are treated by identical formulae. Fourth, the inclusion of an interaction for the pair (AC) introduces terms of somewhat different

energy dependence. In addition, the bookkeeping of various exchange effects (including heavy stripping) becomes simplified in terms of two-cluster expansions of the nuclear states.

It is hoped that this approach to the direct interactions might allow a straightforward extension to include the effects of distortions. A first extension will not introduce any new parameters nor any new interactions; the distortions should be attributable to the interactions that produce the reaction. There is a significant philosophical change in considering always a three-body problem, in that the distortions will depend not on the final nuclear state considered, but rather on the specific clustering of this final state. Thus there is built into this approach a mechanism to allow the distorting parameters to be different for different reactions involving the same nuclear state.

3. Plane Wave Theory

We assume that nonrelativistic quantum mechanics is adequate, so that the reaction cross section in relative coordinates is given by

$$\frac{d\sigma}{d\Omega} = \frac{M_i M_f}{(2\pi \hbar^2)^2} \frac{K_f}{K_i} |R_{fi}|^2 \qquad (2)$$

where R_{fi} is the matrix element of the reaction matrix, connecting states which behave asymptotically as plane waves with definite wave

vectors. The expression (2) gives us the kinematic factors multiplying the square of the matrix element, which involves the reduced masses, M_i and M_f, and the wave numbers K_i and K_f, of the initial and final relative motions. All that remains is for the theory to predict a form and magnitude for the reaction matrix element R_{fi}.

We start from an exact expression for the reaction matrix element, written in terms of the exact Hamiltonian of the whole system, and the truncated Hamiltonians which define the asymptotic forms of the initial and final states. The derivation may be found in the literature (Messiah 61). The truncated Hamiltonians neglect the interactions between the clusters which are not bound; in the initial state, we neglect V_{bc} and V_{ac} but keep V_{ab}; in the final state, we neglect V_{ab} and V_{ac} but keep V_{bc}.

Total Hamiltonian: $T + V_{ab} + V_{bc} + V_{ac}$

Initial Hamiltonian: $T + V_{ab}$

Final Hamiltonian: $T + V_{bc}$.

If we denote the wavefunctions of the truncated Hamiltonians by φ_{ab} and φ_{bc}, and the exact wavefunctions of the total system by $\psi^{(+)}_{ab}$ and $\psi^{(-)}_{bc}$, the reaction matrix is given by either of the expressions

$$R_{fi} = (\psi^{(-)}_{bc} \mid V_{bc} + V_{ac} \mid \varphi_{ab}) \qquad (3a)$$

$$= (\varphi_{bc} \mid V_{ab} + V_{ac} \mid \psi^{(+)}_{ab}) . \qquad (3b)$$

In order to make actual calculations, it will always be necessary to assume a particular form for the wavefunctions of the bound states. For many estimates using a plane-wave theory, harmonic-oscillator wavefunctions are particularly simple to deal with. For more precise calculations, an exponential rather than Gaussian decay may be preferable at large separations. The Hulthen form

$$X(r) = N\left(e^{-sr} - e^{-tr} \right)/r \qquad (3c)$$

is useful for s-states. Whatever choice is convenient or acceptable, the wavefunctions of the truncated Hamiltonians can be written as a product of the bound state wavefunction and a plane wave for the relative motion. Because we deal explicitly with three particles, it is more convenient for our purposes to use the actual masses (not the reduced masses), and not relative velocities, but velocities relative to the center of mass system, in writing down these wavefunctions. Also, for convenience we set $\hbar = 1$, so that the wave vector and momentum vector are the same. Initially, the bound system (AB) moves with wave vector $\underset{\sim}{k}$, and target C moves with opposite momentum $-\underset{\sim}{k}$. The initial relative motion of the bound system is given by a bound-state wavefunction X_{ab}. Thus we have for the asymptotic form of the initial state

$$|\varphi_{ab}) = e^{-i\underset{\sim}{k}\cdot\underset{\sim}{r}_c}\, e^{i\underset{\sim}{k}\cdot(m_a\underset{\sim}{r}_a + m_b\underset{\sim}{r}_b)/(m_a + m_b)}\, X_{ab}(\underset{\sim}{r}_a - \underset{\sim}{r}_b) \qquad (4a)$$

The final state involves an internal wavefunction X_{bc} and a different momentum vector $\underset{\sim}{q}$.

$$(\varphi_{bc}| = e^{-i\underset{\sim}{q}\cdot\underset{\sim}{r}_a} e^{i\underset{\sim}{q}\cdot(m_b\underset{\sim}{r}_b + m_c\underset{\sim}{r}_c)/(m_c + m_b)} X^*_{bc}(\underset{\sim}{r}_c - \underset{\sim}{r}_b) \qquad (4b)$$

In the general case that the clusters are endowed with a spin, these wavefunctions will be multiplied by appropriate spinors $|JM)$ to specify the angular momentum and its projection.

The essential character of the angular distributions is already contained in the particular form we have written for the initial and final states, simply because the states we deal with are not orthogonal. In the plane-wave approximation, we take the asymptotic forms to be valid everywhere, so that the matrix element is an overlap between the functions (4a) and (4b), weighted with the interactions $V_{bc} + V_{ac}$, for example. It is convenient to rewrite the wavefunctions so that they are expressed in terms of coordinates relative to the exchanged particle. At the same time we may observe how symmetric these wavefunctions look, so that it seems quite artificial to introduce an arbitrary cutoff for the integral at the surface of the cluster C.

$$|\varphi_{ab}) = e^{-i\underset{\sim}{k}\cdot(\underset{\sim}{r}_c - \underset{\sim}{r}_b)} e^{i\underset{\sim}{k}\cdot(\underset{\sim}{r}_a - \underset{\sim}{r}_b)m_a/(m_a + m_b)} X_{ab}(\underset{\sim}{r}_a - \underset{\sim}{r}_b) \qquad (5a)$$

$$(\varphi_{bc}| = e^{-i\underset{\sim}{q}\cdot(\underset{\sim}{r}_a - \underset{\sim}{r}_b)} e^{i\underset{\sim}{q}\cdot(\underset{\sim}{r}_c - \underset{\sim}{r}_b)m_c/(m_c + m_b)} X^*_{bc}(\underset{\sim}{r}_c - \underset{\sim}{r}_b) \qquad (5b)$$

If the interactions V_{bc} and V_{ac} may be assumed reasonably smooth and of a range of the order of decay lengths of the initial and final states, the actual shape of the interaction will not change the form of the matrix element very strongly; we may obtain a qualitative feeling for the angular distributions predicted by simply considering the angle and energy dependence of the overlap between the initial and final states. This overlap is the product of two integrals, which are the Fourier transforms of the bound state wavefunctions. There are two integrations to be done, over the two spaces $(\underset{\sim}{r}_a - \underset{\sim}{r}_b)$ and $(\underset{\sim}{r}_c - \underset{\sim}{r}_b)$. Replacing these coordinates by dummy variables $\underset{\sim}{r}$ and $\underset{\sim}{s}$, we have

$$(\varphi_{bc}, \varphi_{ab}) = \int X_{ab}(\underset{\sim}{r})\, e^{-i\underset{\sim}{r}\cdot\underset{\sim}{P}}\, d^3\underset{\sim}{r} \int X^*_{bc}(\underset{\sim}{s})\, e^{i\underset{\sim}{s}\cdot\underset{\sim}{Q}}\, d^3\underset{\sim}{s} \qquad (6)$$

The vectors $\underset{\sim}{P}$ and $\underset{\sim}{Q}$ are linear combinations of the initial and final momenta $\underset{\sim}{k}$ and $\underset{\sim}{q}$ as follows

$$\underset{\sim}{Q} = \underset{\sim}{q}m_c/(m_c + m_b) - \underset{\sim}{k} \qquad \underset{\sim}{P} = \underset{\sim}{q} - \underset{\sim}{k}m_a/(m_a + m_b) \qquad (7)$$

These vectors represent the change in the linear momentum of the particles A and C, and are the only parameters which are angle and energy dependent in the plane-wave theory. They may always be written by inspection by considering what fraction of the total linear momentum corresponds to a given cluster.

If we assume that the initial and final bound states are eigenstates of the orbital angular momentum, with quantum numbers L_o and

L, we may carry out the integration over the angle coordinates after expanding the exponential factors into spherical harmonics,

$$(\varphi_{bc},\varphi_{ab}) = (4\pi)^2 (-i)^L \; Y_L^{M^*}(\Omega)\, (i)^{L_o} \; Y_{L_o}^{M_o}(P) \; \times$$

$$\int_o^\infty X^*_{bc}(r) \; j_L(\Omega r) r^2 dr \quad \int_o^\infty X_{ab}(s) \; j_{L_o}(Ps)\, s^2 ds \qquad (8)$$

These expressions may be summed over the initial and final magnetic quantum number after taking the square; since the statistical weight of the initial state is $1/(2L_o + 1)$, the sum of the squares of the matrix elements is (except for factors)

$$(4\pi)^2(2L+1)\left[\int_o^\infty X^*_{bc}(r)\, j_L(\Omega r) r^2 dr \quad \int_o^\infty X_{ab}(s)\, j_{L_o}(Ps) s^2 ds\right]^2 \qquad (9a)$$

If we do not sum over the final polarizations, in this simplest case we obtain a correlation between the spin polarization of the residual nucleus and the angular distribution of the outcoming particles; the cross section is proportional to

$$(4\pi)^3 |Y_L^M(\Omega)|^2 \left[\int_o^\infty X^*_{bc}(r) j_L(\Omega r) r^2 dr \quad \int_o^\infty X_{ab}(s) j_{L_o}(Ps) s^2 ds\right]^2 . \qquad (9b)$$

The general characteristics of the matrix element when we include an interaction of somewhat more realistic shape do not change

the answer except in detail; the parameters involved remain the momentum changes $\underline{Q}$ and $\underline{P}$. For example, using the Hulthen form for the wave functions, an exponential interaction potential V_{ab} or V_{bc} would only change the effective decay parameter by an additive constant.

The size of the matrix element depends on two factors. One is the strength of the interaction; the other is the probability that the actual nuclear state we are dealing with should indeed be expressible in terms of the cluster wavefunction we have chosen. This kind of idea leads us to make use of cluster expansion coefficients, defined to be the overlap (jm, X_{ab}), where the state vector $(jm|$ denotes the actual nuclear wavefunction of all the nucleon coordinates, and $|X_{ab})$ denotes the form we have chosen for the calculation. The factor so defined roughly corresponds to the reduced width of the usual theory. However, the value of a reduced width is strongly dependent on the "natural" nuclear radius in the theory. Since no natural definition appears under the present approach, it is preferable to give this factor a different name.

The usual theory, especially as applied to deuteron stripping, transforms away the shape and strength of the interactions responsible for the bound states by using the Schrödinger equation in conjunction with the form chosen for the wavefunction, in order to define what the potential actually is. This procedure is mathematically consistent, but

in essence claims that the second derivative of the wavefunction is well known. For the case of deuteron stripping, this procedure has led to adequate predictions of angular distributions with Hulthen wavefunctions, in spite of the fact that these entirely neglect the possibility that the neutron-proton potentials have a repulsive core; it all goes to show that the angular distributions are not a sensitive function of the shape of the interaction.

The mathematical form of the simplest estimate (9a), which is that of the direct overlap, is already adequate for fitting angular distributions. If we use harmonic-oscillator wavefunctions, the Fourier integrals may be done by inspection, since it is well known that the Hermite orthogonal functions are their own Fourier transforms. The qualitative features of these answers are identical to those of the Butler shapes. When L = 0, in the final state, there is a peak at $Q = 0$ (here, Q is the magnitude of the vector $\underline{Q}$), and the peak moves to higher values of Q with increasing L. If we take our simplest model seriously, the secondary peaks of an L = 0 pattern must be interpreted as being due to admixtures of states of higher radial quantum number in the wavefunction of the final state. We interpret the observed angular distributions as yielding information on the actual radial wavefunctions of the transferred particle in the initial and final states, X^*_{bc} and X_{ab}.

The case of arbitrary spins for the three clusters involved can be done with little work. The matrix element again factors into a radial integral identical to the one we have obtained neglecting the spins, and a factor involving Clebsch-Gordan coefficients and the spherical harmonics, evaluated at the directions defined by the two momentum-change vectors, $\underset{\sim}{Q}$ and $\underset{\sim}{P}$.

If the interactions neglected in the truncated Hamiltonians are weak compared to the energies of the relative motion, the plane wave approximation is justifiable and the correct answer should be obtainable in our model by carrying out the appropriate integrals including the radial dependence of the interparticle interactions, V_{ab}, V_{bc}, and V_{ac}. The most reasonable assumption that leads to calculable matrix elements is that the two-particle interactions are real central scalar potentials. For a stripping problem we may consider the expression corresponding to (3a). In this case we need to compute the matrix elements of the two interactions V_{bc} and V_{ac}.

$$R_{fi} = (\varphi_{bc} | V_{bc} | \varphi_{ab}) + (\varphi_{bc} | V_{ac} | \varphi_{ab}) \qquad (10)$$

We assume that the interparticle potentials depend only on the magnitude of the separation of the pair. Then the matrix element of V_{bc} in (10) factors into the product of a function of $\underset{\sim}{Q}$ and a function of $\underset{\sim}{P}$. The function of $\underset{\sim}{P}$ is the transform of the initial bound state X_{ab}; the function of $\underset{\sim}{Q}$ is the transform of the product of the final bound state

wavefunction and the potential $X^*_{bc} V_{bc}$, which is a folding of the transform of X^*_{bc} with the transform of V_{bc}. For central interactions of reasonable shapes, the qualitative features of the integral will not change greatly from the simplest approximation; we simply expect the bumps to be broader, and the sharp detail to have been lost.

The matrix element of the interaction V_{ac} does not factor in the same way. It is an integral over two coordinates but it may be reduced to an integral over one single variable by transforming into momentum space. We obtain

$$(\varphi_{bc}, V_{ac}\ \varphi_{ab}) = \int \frac{d^3\underset{\sim}{w}}{(2\pi)^3} X^*_{bc}(\underset{\sim}{w}-\underset{\sim}{Q})\, V'_{ac}(\underset{\sim}{w})\ X'_{ab}(\underset{\sim}{w}+\underset{\sim}{P}) \quad (11)$$

where X' is used to denote the Fourier transform of X. There are various limiting cases in which we may readily see that this integral yields a function indistinguishable from those we have considered. If the interaction is long range, then its transform V'_{ac} should be sharp and narrow, and it may be approximately represented by a δ-function; in this case we obtain the "simplest" estimate once again. If at least one of the wavefunctions is (in space) very diffuse, then its transform can also be approximately replaced by a δ-function, and the answer is again in the form of a product of transforms.

It is possible to evaluate analytically integrals such as (11) for at least two types of wavefunctions and shapes of the interaction; for

harmonic-oscillator wavefunctions and Gaussian potentials, or for exponentially decaying wavefunctions and potentials of the Yukawa shape. The angular distributions that are predicted by equation (10) in this way are qualitatively very similar to the Butler curves. The differences lie chiefly in the large-angle behavior; with the present formulae somewhat higher cross sections are predicted for the backward angles. This is in the right direction if we want to obtain fits better than those of the Butler theory for most angular distributions. The reason why our results do not look very different from those of the "surface" theories in the plane wave approximation is that the dominant contribution to the integrals comes from the peripheral region unless the wavefunctions are abnormally large in the interior, because of a resonance.

The preceding considerations suggest that the detailed shape of the angular distributions for direct reactions contains information about the radial wavefunctions of the initial and final states, rather than simply information about the orbital motion in the final state. Thus the reproduction of minor details, such as secondary peaks, is mostly fortuitous. The extraction of the maximum information about the radial wavefunctions will be contingent upon our ability to disentangle the distortion effects, but it is clear that the angular distributions contain something like the transforms of the radial wavefunctions; they are the Fourier transforms in the plane-wave approximation.

4. Exchange Effects

The reaction amplitudes may also contain terms in which the nuclear cluster A which is emitted must be considered to be originally contained as part of the target nucleus. These amplitudes must be added; they interfere with the terms that consider A to be part of the incident projectile particle. In an approach that considers only three bodies, this means that in order to describe the exchange effects we must write reaction amplitudes corresponding to different clusterings of the nucleons. The reactions ordinarily denoted as being of the "stripping" type differ from the other direct reactions (knockout, pickup, heavy stripping, inelastic scattering) only in whether it is the target particle or the projectile particle that is considered to be made up of two clusters; in the stripping reactions, it is the projectile which is considered to be composite.

It is simplest to display the similarities of all direct reactions when viewed as three-cluster processes by means of diagrams specifically identifying the target, projectile, and product particles; we do this in Figure 15 for some of the reactions involving protons or deuterons incident on Li^7 as a target. Since we specifically exclude the possibility that the three clusters form a metastable nuclear state, we have drawn the lines representing the clusters so that three of them

are never together. The diagrams are intended to be useful only in the bookkeeping, emphasizing which particle is to be viewed as the exchanged particle; they are not intended to represent individual matrix elements with interactions represented by vertices; however, they also may be taken as contributions to the reaction matrix element in the sense of dispersion theory (Shapiro 61). In the plane wave approximation we have discussed, the matrix element for each clustering will involve two terms, one for the interaction producing one of the bound pairs, and another for the interaction V_{ac}, between particles which are never bound to each other (Figure 15).

If we allow only the exchange of a single cluster, a reaction such as the (d, p) reaction may occur in two ways, which are ordinarily termed stripping and heavy stripping. The initial and final states involved are in principle quite different with our description, since in the heavy stripping the deuteron is captured as a single chunk, instead of dissociating. The heavy-stripping term is always "backward peaked" from the point of view of the (d, p) reaction only because the momentum changes of the core particles, $\underset{\sim}{Q}$ and $\underset{\sim}{P}$, involved different combinations of the momenta of the incoming deuteron and outgoing proton. We list the definitions of the parameters $\underset{\sim}{Q}$ and $\underset{\sim}{P}$ for both cases, in terms of the momenta of the incoming deuteron $\underset{\sim}{k}$ and the outgoing proton $\underset{\sim}{q}$, and in terms of the masses of proton, neutron, deuteron, and target.

Ordinary Stripping: $\underset{\sim}{Q} = \underset{\sim}{q}m_t/(m_t + m_n) - \underset{\sim}{k}$, $\quad \underset{\sim}{P} = \underset{\sim}{q} - \underset{\sim}{k}m_p/(m_p + m_n)$

Heavy Stripping: $\underset{\sim}{Q} = \underset{\sim}{q}m_d/(m_t + m_d) + \underset{\sim}{k}, \quad \underset{\sim}{P} = \underset{\sim}{q} + \underset{\sim}{k}m_p/(m_p + m_t)$

The backward peaking occurs because the matrix elements are usually largest when the magnitudes of the vectors $\underset{\sim}{Q}$ and $\underset{\sim}{P}$ are small. For ordinary stripping, this occurs for $\underset{\sim}{k}$ and $\underset{\sim}{q}$ parallel; for heavy stripping, this occurs for $\underset{\sim}{k}$ and $\underset{\sim}{q}$ antiparallel. In the three-body viewpoint, there are no statements that can be made a priori about whether the heavy stripping contribution to the cross section will be large relative to the ordinary stripping part. Each will depend on the relative strengths of the effective intercluster potentials and on the values of the cluster expansion coefficients; these parameters are presumably independent. There is, however, a connection between the results of different reactions, when they involve the same pairs of clusters. For example, in Figure 15 we see that the reaction $Li^7(d,p)$ and the pickup $Li^7(p,d)$ involve the proton-neutron interaction; the knockout $Li^7(p,n)$ and the pickup $Li^7(p,d)$ involve the same Li^6-neutron interaction; the inelastic scattering $Li^7(p,p')$ and the heavy stripping $Li^7(d,p)$ may involve the same He^6-proton interaction.

5. Small Distortions

The simplest estimate, using the direct overlap as the form of the matrix element, may be used in order to estimate the effects of distortions of the relative motions. Since the plane-wave theory often

gives good fits, it seems appropriate to investigate the changes induced by including the second order terms of the Born approximation for the wavefunctions. Clearly, there must be some energy region in which this is a meaningful procedure. Using Hulthen wave functions, and distorting potentials of the Yukawa shape, it is possible to obtain analytic expressions for the direct overlap, but these are rather unwieldy and do not result in expressions convenient for application to the problem at hand. The results are, however, suggestive of extremely simple procedures for estimating the possible effects of distortions.

For some of the problems to which the theory might be applied, the Born series may begin to converge at bombarding energies as small as 5 MeV; there is, therefore, some justification in considering that the second order terms may give corrections of the right trend at useful energies.

The most prominent effect on the angular distributions is due to an enhancement of the wave function near the origin for attractive potentials, or a diminution of the amplitude for repulsive potentials. An analytic estimate of distortion effects which has a form very like the results of the second order Born approximation may be simply obtained by introducing a penetration factor of such form that the integrations can be carried out; for use with harmonic-oscillator wavefunctions a suitable factor may be $(1 - G(E) \exp(-r^2/a^2))$, where $G(E)$ is small for large bombarding energies and becomes of the order

of l at energies such that the Born series begins to diverge. This kind of penetration factor reproduces the backward peaks which have often been observed in stripping reactions for which the heavy stripping contribution was suspected to be small, but for which distortion effects may be important. It is of interest to note that the forward angles are considerably diminished in amplitude, but the shape is likely to remain largely undisturbed.

This estimate goes a long way toward confirming our guess that the shape of the angular distributions at forward angles is insensitive to moderate distortions. A qualitatively similar conclusion has been reached by Elton and Jackson (Elton 62) after examining the results of a series of numerical calculations using W.K.B. wavefunctions for the relative motions.

The preceding estimates were conceived in order to have some idea for the justification of the use of a plane-wave theory in interpreting the results of our experiment. For the bombarding energies used, there is little hope that the effective intercluster potentials should be weak compared to the kinetic energies. The best that can be done is to note that B^9 is unbound with respect to proton emission, so there is some hope that the average distortion of the motion of the emergent proton in the field of a Be^8 cluster may be due to an average potential which may be relatively weak.

V. DISCUSSIONS AND CONCLUSIONS

The theory described in the previous sections, in its simplest plane-wave form, has been used in an attempt to interpret the angular distributions of the reaction $Li^6(He^3,p)Be^{8*}$. For the case of the level "A" at 16.63 MeV excitation, the general shape of the angular distributions suggested capture into an s-state. Unfortunately, the errors assigned to the experimental points are too large to define a suitable fit within narrow limits, so that no claim may be made that the fit is unique.

We have chosen the Hulthen wavefunction (IV.3c) as the likeliest shape for wavefunctions of bound states with L = 0; the theoretical form of the function defining the angular distribution is in this case

$$R_{fi} = W\left[1/(Q^2+\alpha^2) - 1/(Q^2+\beta^2)\right]\left[1/(P^2+\gamma^2) - 1/(P^2+\delta^2)\right], \quad (1)$$

where the parameters involved are an amplitude constant W and four decay parameters α, β, γ, δ, which are inverses of the various decay lengths. The variables are Q and P, which are the magnitudes of the vectors defined by equation (IV.7). The smallest of the decay parameters may be estimated from the binding energies of the clusterings considered. For example, the binding energy of a deuteron and

Li^6 is near 5.5 MeV for an excitation of 16.63 in Be^8; the binding energy of a proton in He^3 is 5.2 MeV. The decay parameters are the inverses of the wave numbers corresponding to bound states of this energy. The values are

$$\alpha = 0.628 \text{ Fm}^{-1} \qquad \text{(Decay Length = 1.65 Fm)}$$

$$\gamma = 0.407 \text{ Fm}^{-1} \qquad \text{(Decay Length = 2.48 Fm)}$$

The value of the parameter that best seems to fit the angular distributions at all energies is the following

$$\alpha = 0.675 \text{ Fm}^{-1} \qquad \text{(Decay Length = 1.48 Fm)}$$

The value of the He^3 decay length has not been adjusted. The inner decay lengths $1/\beta$, $1/\delta$, have not been adjusted, but simply chosen to be equal to one fourth of the outer decay lengths; this inner decay parameter makes very little difference in the shape of the angular distribution, provided it is larger than the outer decay parameter by a factor of three or more. The theoretical curves shown in Figures 10, 11, 12, 13 and 14 have been obtained in this manner.

For the angular distribution of the level B at 16.94 MeV excitation, the hint of a dip at forward angles and of a maximum near 40° suggests that if one insists on interpreting the result in terms of a stripping theory, the final state wavefunction ought to be of an L = 2 character. In order to make use of the simplest estimate, we have assumed the radial wavefunction to be of the form

$$X_{bc}(s) = Y_2\, s^2\, e^{-ws} \tag{2}$$

which is the form of the first L = 2 hydrogenlike wavefunction. The angular distribution is then proportional to the square of the radial integral

$$I(w,Q) = \int_0^\infty s^2\, e^{-ws}\; j_2(Qs)\, s^2\, ds \tag{3}$$

$$I(w,Q) = \frac{48\, w\, Q^2}{(w^2 + Q^2)^4} \tag{3a}$$

which can be easily done by writing $j_2(Qs)$ in terms of sines and cosines. The matrix element is then

$$R_{fi} = W' \left[\, 1/(P^2 + \gamma^2) - 1/(P^2 + \delta^2) \,\right] I(w,Q) \quad . \tag{4}$$

The theoretical curves shown in Figures 10, 11, 12, 13 and 14 for the level B have been obtained in this manner. The parameter w is the inverse of a decay length corresponding to the binding energy; for the curves drawn in the figures it has the value

$$w = 0.550\ \mathrm{Fm}^{-1} \qquad \text{(Decay Length = 1.82 Fm)}$$

The conclusion is that the angular distributions of the reactions may be adequately explained with a model which assumes that a deuteron is captured as a single lump into an orbit about Li^6 as a core. If a plane-wave theory may be expected to give the shape of the

angular distributions correctly, the deuteron is captured into an L = 0 orbit to make up the level at 16.63 MeV, and it is captured into an L = 2 orbit to make up the level at 16.94 MeV.

This information is sufficient to suggest a spectroscopic assignment for the levels, provided we assume that the recognition of an L = 2 pattern means that an L = 0 capture is forbidden. The level at 16.94 should be 4^+; if it were 2^+ or 0^+, it could be formed by an L = 0 deuteron. The level at 16.63 MeV might be 0^+ or 2^+; it evidently is a good candidate to be the $J = 2^+$ analog of the ground states of Li^8 and B^8.

The magnitudes of the cross sections may also be explained qualitatively with these spectroscopic assignments. The matrix element for captures into L = 2 orbits are commonly smaller than matrix elements for capture into L = 0 orbits by a significant factor; it is not uncommon to find them to differ by an order of magnitude. The observed cross sections in this case are nearly the same size because of the isotopic spin selection rule. Since both reactions apparently proceed through capture of a $J = 1^+$, T = 0 deuteron by a $Li^6(J = 1^+, T = 0)$ core, the production of the 16.63 MeV level ($J = 2^+$, T = 1) is inhibited, whereas the production of the 16.94 level ($J = 4^+$, T = 0) is not.

These assignments, for level B in particular, are made in the spirit of attempting to give an account of the present results with the simplest available model. It becomes quite clear, after a perusal of the figures, that the evidence on level B does not define a pattern which is interpretable with great confidence. More positive conclusions may be possible after refined measurements of the cross sections are made, especially at small angles.

APPENDIX A

On the Kinematics of a Two-Stage Nuclear Reaction. The Spectrum from the Secondary Breakup.

In this Appendix we turn our attention to a calculation of the spectral shape to be expected for the alpha particles coming from the breakup of highly excited sharp levels of Be^8. The process is considered to occur in two well-defined steps. First, we have the production of Be^{8*} with a definite excitation energy, that is, with a definite energy release which we denote as Q'.

$$Li^6 + He^3 \longrightarrow Be^{8*} + p \; ; \; Q' . \qquad (A.1)$$

This is followed by the breakup of Be^8, considered as a system isolated from all other particles.

$$Be^{8*} \longrightarrow \alpha_1 + \alpha_2 \; ; \; Q'' . \qquad (A.2)$$

The general case of the breakup of broad levels may be considered as a superposition of these processes, occurring with different probabilities, depending on the value of Q' (Phillips 60). The value Q'' of the second breakup is, of course, restricted by the energy release which describes the overall process

$$Li^6 + He^3 \longrightarrow p + He^4 + He^4 \qquad (A.3)$$

$$Q' + Q'' = 16.881 \text{ MeV} .$$

There is no possibility of interference between breakups corresponding to different values of Q', since the energy of the emergent particle in the first breakup uniquely determines the value of Q'.

A nonrelativistic treatment will be given. If we observe particles at a definite angle θ relative to the incoming beam, the velocity of the alpha particles in the laboratory is simply the vector sum of three velocities.

1. $\underset{\sim}{u}$, the velocity of the $(Li^6 + He^3)$ system in the laboratory,
2. $\underset{\sim}{v}$, the velocity of the Be^{8*} relative to the $(Li^6 + He^3)$,
3. $\underset{\sim}{w}$, the velocity of an alpha particle relative to the Be^{8*}.

We are interested in computing the spectrum, the probability distribution $W(g)$, at a fixed angle of observation θ, where g is the vector sum

$$\underset{\sim}{g} = \underset{\sim}{u} + \underset{\sim}{v} + \underset{\sim}{w} \ . \qquad \text{(A.3')}$$

We need only consider a discrete value of Q'. Once Q' is given, the equations expressing the conservation of energy and momentum can be used to yield definite discrete values of the magnitudes u, v, w, if we specify the bombarding energy. For concreteness, we use in our example notation appropriate to our reaction $Li^6(He^3,p)Be^8$, although, of course, the mathematics is identical for any two-stage reaction. We have, in terms of the laboratory

bombarding energy E_L (and in units such that c = 1),

$$u = \left[M(He).2.E_L \right]^{\frac{1}{2}} / \left[M(He) + M(Li) \right] \quad . \tag{A.4a}$$

In terms of the center of mass energy $E = E_L . M(Li)/[M(Li) + M(He)]$, we have

$$v = \frac{M(p)}{M(p) + M(Be)} \left[\frac{2.(E+Q').[M(p)+M(Be)]}{M(p).M(Be)} \right]^{\frac{1}{2}} \tag{A.4b}$$

And in terms of the energy release Q'' of the second breakup,

$$w = \left[2.Q'' / [M(\alpha) + M(\alpha)] \right]^{\frac{1}{2}} \tag{A.4c}$$

The probability of observing a given magnitude of $\underset{\sim}{g}$ at a given angle in the laboratory is then the integrated probability that the vectors $\underset{\sim}{v}$ and $\underset{\sim}{w}$ add up to give $(\underset{\sim}{g} - \underset{\sim}{u})$. This can happen when the tip of $\underset{\sim}{v}$ lies in a circle about the direction of $(\underset{\sim}{g} - \underset{\sim}{u})$, as may be seen in Figure 16.

We note that the angle between $\underset{\sim}{w}$ and $\underset{\sim}{v}$ is constant, and that the angle between $\underset{\sim}{u}$ and $\underset{\sim}{v}$ is restricted to a definite range, which in general will be smaller than $(0 - - \pi)$. We also see that it will be necessary to integrate over an azimuthal angle φ, between the limits $(0 - - 2\pi)$.

We may now proceed to write the relations between the vectors that will lead to specific mathematical expressions for the probabilities.

We first deduce the restrictions in terms of δ-functions. The relation (A.3') is squared, to give

$$g^2 = u^2 + v^2 + w^2 + 2uv\cos(uv) + 2vw\cos(vw) + 2uw\cos(uw)\cos(vw) + 2uw\sin(uv)\sin(vw)\cos\varphi \qquad (A.5a)$$

For economy of writing, we will let

$$x = \cos(uv)$$

$$y = \cos(vw)$$

$$z = \cos\theta \quad \text{(the laboratory angle)},$$

so that the previous equation is written as

$$g^2 = u^2 + v^2 + w^2 + 2uvx + 2vwy + 2uwxy + 2uw\cos\varphi\sqrt{(1-x^2)}\sqrt{(1-y^2)} \qquad (A.5b)$$

The second restriction is obtained by setting $\underset{\sim}{u}\cdot\underset{\sim}{g}$ constant; we write

$$\underset{\sim}{u}\cdot\underset{\sim}{g} = ugz = u^2 + uvx + uwxy + uw\cos\varphi\sqrt{(1-x^2)}\sqrt{(1-y^2)}\,. \qquad (A.6)$$

These two relations (A.6) and (A.5b) have been written so they define the quantities g and z in terms of the variables that we wish to integrate over, which are x, y, and φ. Since only $g > 0$ is of physical interest, we introduce the change of variables as a delta function written as follows

$$\delta(g - g(xy\varphi)) = 2g\,\delta(g^2 - g^2(xy\varphi)) \qquad (A.7)$$

The second restriction we may use as a δ-function written as

$$\delta(z - z(xy\varphi)) = g\,\delta(gz - gz(xy\varphi)) \qquad (A.8)$$

The combined factor expressing the restrictions is therefore

$$\delta(g - g(xy\varphi))\,\delta(z - z(xy\varphi)) =$$

$$2g^2\,\delta(g^2 - g^2(xy\varphi))\,\delta(gz - gz(xy\varphi)) \qquad (A.9)$$

The function giving the probability distribution of the magnitude of g at fixed z is now given by integrating over the probability distribution of the variables x, y, and φ, subject to the restriction (A.9)

$$W(g,z) = \int_{-1}^{+1} dx \int_{-1}^{+1} dy \int_{0}^{2\pi} d\varphi\; W_o(x)\, W'(y,\varphi)\, 2g^2\, \delta(g^2 - g^2(xy\varphi))\, \delta(gz - gz(xy\varphi)) \qquad (A.10)$$

If no spin polarizations are measured, the distribution W' has no dependence on the azimuthal angle φ. Since the reaction occurs in two stages by hypothesis, we write the probabilities of the two breakups independently. We may do the integration over the coordinate y first; dropping constants which appear as factors, we first eliminate cos φ from equation (A.5b) by use of equation (A.6); we let

$$y_o = (g^2 - v^2 - w^2 + u^2 - 2ugz)/2vw\ , \qquad (A.11)$$

then; $W(g,z) = 0$ if $|y_o| > 1$; otherwise, the expression is

$$W(g,z) = \int_{-1}^{+1} dx \int_{0}^{2\pi} d\varphi\; W_o(x)\, W'(y_o,\varphi)\, \frac{2g^2}{2vw}\, \delta(gz - u - vx - wxy_o - w\cos\varphi \sqrt{(1-x^2)}\sqrt{(1-y_o^2)}) \qquad (A.12)$$

Next, we do the integration over the coordinate φ. In the

range $0 < \varphi < 2\pi$, $\cos^{-1}\varphi$ is double valued, and the δ-function in principle will give contributions from both values. If, however, we assume that $W'(y)$ has no φ dependence, or that the dependence is on $\cos\varphi$ rather than on φ, these terms combine, and we arrive at the following general expression for $W(g,z)$:

$$W(g,z) = \int_{-1}^{+1} dx\, W_o(x)\, W'(y_o,\varphi_o)\, \frac{2g^2}{2vw}\, \frac{1}{w\sqrt{(1-x^2)}\,\sqrt{(1-y_o^2)}}\, \frac{1}{\sin\varphi_o} \qquad (A.13)$$

where

$$\varphi_o = \cos^{-1}\left[(gz-u-vx-wxy_o)/w\,\sqrt{(1-x^2)}\,\sqrt{(1-y_o^2)}\right] \qquad (A.14)$$

The restriction $|\cos\varphi_o| \leq 1$ for real φ_o means that the integrand of (A.13) is zero unless the denominator is real. Therefore we may express $W(g,z)$ as an integral, not necessarily between limits -1 to +1, but between the two values of x which make the denominator zero. This will hold if these two values lie between -1 and +1. However, physical values of x are also limited to those for which $|x^2| \leq 1$, if the parameters u, v, g represent physical velocities. For the particular case at hand, we may write simply

$$W(g,z) = \int_{\underline{x}}^{\bar{x}} dx\; \frac{2\,W_o(x)\;\; W'(y_o,\varphi_o)}{\left[w^2(1-x^2)(1-y_o^2) - \left[(gz-u)-(v+wy_o)x\right]^2\right]^{\frac{1}{2}}} \qquad (A.15)$$

where the limits $\underline{x}$ and $\bar{x}$ are the solutions to the quadratic equation obtained by setting the denominator equal to zero. In order to carry out the integration, we shall need to group the denominator into terms in order of descending powers of x. If at the same time we write y_o in terms of the quantities g, u, v, w, and z,

$$A(g,z) = \frac{2g^2}{vw} \int_{\underline{x}}^{\bar{x}} \frac{W_o(x)\ W'(y_o,\varphi_o)\ dx}{\sqrt{(ax^2 + bx + c)}} \tag{A.16}$$

where
$$a = -(g^2 + u^2 - 2ugz)$$
$$b = (gz-u)\,(g^2 + u^2 - 2ugz - w^2 - v^2) \tag{A.17}$$
$$c = w^2(1-y_o^2) - (gz-u)^2$$

The fact that the integration is to be carried out between limits which are zeros of the denominator means that the integrated expressions achieve a manageable simplicity in certain cases. Assuming that $W_o(x)$ is adequately represented by a power series

$$W_o(x) = 1 + \alpha x + \beta x^2 + \gamma x^3 \ldots \tag{A.18}$$

we may carry out the integration explicitly. Keeping only three powers of x, we eventually arrive at the result

$$W(g,z) = \frac{g^2}{vw}\, W'(y_o)\, \frac{1}{\sqrt{(-a)}} \left[1 + (-b/2a)\alpha + \frac{(3b^2-4ac)\beta}{8a^2} + \left(\frac{3bc}{4a^2} - \frac{5b^3}{16a^3}\right)\gamma \ldots\right] \tag{A.19}$$

where the parameters a, b, c are defined in (A.17). We summarize this result in terms of the parameters u, v, w, g, and z for the simplest cases, which are of interest in connection with this experiment. We neglect any nonisotropic distribution of the secondary breakup.

I. The spectrum to be expected from two isotropic breakups is

$$W_I(g,z) = g^2 / \left[vw \sqrt{(g^2 + u^2 - 2ugz)} \right] \qquad (A.20)$$

II. If the first breakup has an asymmetry proportional to $(1+\alpha x)$, and the second breakup is isotropic,

$$W_{II}(g,z) = W_1(g,z) \left[1 + \alpha \frac{(gz-u)(g^2+u^2-2ugz-w^2+v^2)}{2v(g^2+u^2-2guz)} \right] \qquad (A.21)$$

These algebraic forms are expected to be valid between the maximum and minimum values of g allowed by the conservation laws. These limits are obtained by setting y_o equal to +1 and -1, respectively, corresponding to a parallel or antiparallel alignment of the vectors $\underset{\sim}{v}$ and $\underset{\sim}{w}$. In terms of the laboratory angle θ and the velocities u, v, w given by the equations (A.4abc), the maximum and minimum values are given by

$$g = u\cos\theta + \sqrt{(h^2 - u^2 \sin^2\theta)} \qquad (A.22)$$

where $h = v + w$ when $y_o = +1$, and $h = v - w$ when $y_o = -1$.

It is formulae (A. 20) and (A. 21)that have been used in deducing the theoretical curves for the interpretation of the alpha-particle spectra, shown in Figure 7.

The distribution $W'(y_o)$ appears as a factor in (A. 19), so that information about the second breakup is in principle readily accessible if one has measured the angular distribution of the first breakup, and the alpha-spectrum, with sufficient accuracy. For the present experiment the additional complexities introduced by the presence of two levels preclude any unique interpretation of the data.

APPENDIX B

Methods and Formulae for the Data Reduction

1. Calibrations of the Spectrometer

The energy of the incoming particles has been calculated in terms of the electrostatic analyzer calibration constant k_e as follows

$$E = E_o (1 + E_o / 2Mc^2) \qquad \text{with } E_o = Z\, k_e\, V_{esa} . \qquad \text{(B. 1)}$$

M is the mass of the ion whose energy is being analyzed, Z is its charge number, and k_e is the constant 0.434092, calculated from the measurements of Bardin (Bardin 61); V_{esa} is the potentiometer setting required to balance the bridge circuit which measures the potential difference between the plates of the electrostatic analyzer.

The energy of an elastically scattered particle has been calculated in terms of the incident energy by means of the relation

$$E(\text{scat}) = F^2 \cdot E(\text{incident})$$

$$\text{with } F = \frac{\sqrt{(M_1 M_3)}\cos\theta}{(M_3 + M_4)} + \left[\frac{M_4 - M_1}{M_3 + M_4} + \frac{M_1 M_3 \cos^2\theta}{(M_3 + M_4)^2} \right]^{\frac{1}{2}} \qquad \text{(B.2)}$$

We use the notation with subscripts 1, 2, 3, 4 as in Marion (Marion 61) and Schiff (Schiff 55); particle 1 is the projectile, 2 is the target, 3 is

the emergent light particle, and 4 is the residual nucleus; θ is the lab angle between the momenta (1, 3).

The corrections for relativistic effects have been neglected. They are largest for protons, for which they are of the order of 1 part in 2000. To calculate the spectrometer calibration, we have assumed that the midpoint of the rise of a profile such as is shown in Figure 5 corresponds to the energy E(scat). The spectrometer constant k_m has been determined from the equation

$$E(\text{scat}) = E_o\,(1 - E_o/2Mc^2) \quad \text{with } E_o = k_m Z^2 M_p/(MI_o^2) \qquad (B.3)$$

where M_p is the mass of the proton, measured in the same units as the ionic mass M; the fluxmeter setting corresponding to the midpoint of the rise of the profile is I_o. The constants k_m are listed in Table I.

2. Stopping Cross Sections

We have used for calculations of energy losses the values of proton stopping cross sections ϵ_p as given by the Bloch formulae with constants suggested by W. Whaling (Whaling 58)

$$\epsilon_p = (C_1/E_p)\left[\ln(E_p/Z) + C_2\right] \quad \text{Mev-cm}^2 \text{ per } 10^{18} \text{ atoms} \qquad (B.4)$$

with the following values for the constants C_1 and C_2

	C_1	C_2	
For lithium	0.000718	4.69	
For copper	0.00695	5.21	(B.5)
For tungsten	0.0176	5.22	

These values for the tungsten constant have been obtained by a linear extrapolation of the gold and lead constants using Z as a variable.

The proton energy E_p is in Mev and Z is the atomic number of the stopping material. The stopping cross sections for He^3 ions have been obtained from the proton stopping cross sections by assuming that ϵ for He^3 of energy E is 4 times ϵ_p at energy E/3 (Whaling 58). The Bloch formula is sufficiently accurate for the purposes of this experiment at the bombarding energies used.

3. Determination of the Instrumental Constant

This constant is measured by comparing a known cross section to its measured value. The known cross section is Rutherford scattering of an incident proton or He^3 from a copper or tungsten target. The Rutherford cross section has been calculated as

$$\frac{d\sigma(E')}{d\Omega} = \left[Z_1 Z_2 e^2 / \left[4 E' \sin^2(\theta/2) \right] \right]^2 \quad Fm^2 \qquad (B.6)$$

with $e^2 = 1.440$ Mev-Fm; E' is the center of mass energy in MeV, and θ is the center of mass angle.

The cross section is measured in terms of the yield (number

of counts) at an energy E_{20} as given by the magnetic spectrometer setting

$$\frac{d\sigma(E)}{d\Omega} = \frac{K\,N}{E_{20}} \left[\epsilon(E_{10})\, F + \epsilon(E_{20}) \cos\theta_i / \cos\theta_f \right] \qquad (B.7)$$

where N = Yield

F = Constant defined in (B.2)

E_{10} = Incident energy as given by the electrostatic analyzer calibration (B.1)

E_{20} = Exit energy as given by the magnetic spectrometer calibration (B.3)

K = Instrumental Constant

θ_i = angle of incidence (beam to target normal)

θ_f = exit angle (target normal to spectrometer acceptance)

The center of mass energy is that corresponding to E, which is the actual energy at which scattering takes place, and is approximately given in terms of the analyzer energy and the spectrometer energy by the relation

$$E = \frac{E_{20}\,\epsilon(E_{10}) \cos\theta_f + E_{10}\,\epsilon(E_{20}) \cos\theta_i}{\epsilon(E_{10}) \cos\theta_f + \epsilon(E_{20}) \cos\theta_i} \qquad (B.7a)$$

The instrumental constant K is compared to the nominal value which it would have it we take previous measurements in this laboratory as being still applicable; the definition is

$$K = Z\, e\, R\, \varphi / 2\, C\, V\, \Omega_L \qquad \text{(B.7b)}$$

where Z = charge number of incident ions

$e = 1.60206 \times 10^{-19}$ coulomb

R = resolution of spectrometer (assumed to be 231 for 1/4 inch slit)

C = capacitance of capacitor

V = firing voltage of beam current integrator

Ω_L = solid angle of spectrometer (0.0063 Steradians)

φ = detection efficiency (= 1 in this experiment)

The atomic stopping cross sections have been obtained from the formulae (B.5). In the case of tungsten, it has been necessary to estimate a correction factor by reading the graphs given by Whaling (Whaling 60) for the ratio of the expected cross section to the observed stopping cross section when the parameter E/Z is very small. The measurements of the instrumental constant are summarized in Table II.

4. Q Values

We have used the nonrelativistic formula defining the Q value in a nuclear reaction. (The notation with subscripts 1, 2, 3, and 4 is explained after equation (B.2)):

$$Q = \frac{M_3 + M_4}{M_4} E_3 - \frac{M_4 - M_1}{M_4} E_1 - \frac{2\sqrt{(M_1 M_3 E_1 E_3)}}{M_4} \cos\theta \qquad \text{(B.8)}$$

The energy E_1 of the incident particle has been assumed to be given by (B.1), and the energy E_3 of the emergent light particle has been assumed to be given by equation (B.2), both corrected for their average energy loss in the target.

5. Cross Sections from a Thin Target

The expression giving the cross section from a thin target may be deduced to be

$$\frac{d\sigma}{d\Omega} = \frac{Z\, e\, R}{C\, V\, \Omega_L (nt)} \int \frac{N(I)}{I}\, dI \qquad (B.9)$$

where N(I) is the number of counts recorded at a fluxmeter setting I; the other symbols are defined in (B.7b), except (nt), which is the target thickness, in atoms/cm^2, in the direction of the incident beam.

6. Determination of the Cross Sections

The differential cross sections are to be obtained from the formula (B.9). The integration has not been performed directly from the actual distribution of counts N(I); first, the distribution has been converted to the Q value as a variable, by means of the relations (III.2.3). The resulting Q value spectra have then been fitted by a curve of the following algebraic form

$$W(Q) = \frac{M\, G^2}{(Q - A)^2 + G^2} + \frac{M' G'^2}{(Q - B)^2 + G'^2} + C\,. \qquad (B.10)$$

The cross sections are then given by the products, πGM and $\pi G'M'$.

The fitting was done with the help of a computer program. The raw data consisted of a table of counts versus spectrometer settings, with the electrostatic analyzer setting, spectrometer angle, target orientation angles, slit size, capacitance of capacitor, and target thickness. First the computer constructed a table of differential cross section as a function of Q value; this involves the use of equation (B.9) together with (B.8) and the conversion equations (III.2.3); at the same time the computer made appropriate target-thickness corrections. The curve fitting was done by a least-squares method. Although there are seven parameters in the shape assumed for the Q value spectra (B.10), not all of them were adjusted in every spectrum individually; for example, the parameter (A - B) was kept fixed in each individual fit, but chosen so as to give the best over-all fit in all spectra. The parameters G and G' were not adjusted, but chosen by quadratically combining a natural width G_o or G'_o with the instrumental and target-thickness widths expected. The instrumental widths were the spectrometer resolution in both energy and angle, converted to Q value widths by partial differentiation of (B.8). The widths G_o and G'_o were chosen so as to give the best over-all fit, in all spectra simultaneously.

The fit of the linear parameters M, M', and C was done by successively adjusting each one to give the smallest "squares" sum. Initial guesses were made from the magnitudes of the largest and

smallest values of the experimental cross sections as functions of the Q value. The points were weighted inversely as the square of the statistical error; it was assumed that the error in N(I) was $\sqrt{N(I)}$. As a criterion for the goodness of a fit, we have used the square root of the sum of the squares of the differences between the experimental values and the fitted values given by (B. 10), divided by the statistical errors, and then normalized by dividing by the number of points less the number of adjustable parameters. For a large number of points, this criterion is equivalent to the "Chi-Square" method; the most favored value of our parameter should be 2.0 if we are using the correct curve for the fit. The average and variance of the values of this parameter in the fits of 78 spectra was 2.4 ± 1.1.

The parameter A was adjusted by a cut-and-try method, taking steps of 2 kilovolts, after each adjustment of the linear parameters.

It was found that by this method of successive adjustment of one parameter at a time, rather than all parameters simultaneously, it was less likely for the program to find an unphysical set of parameters as the "best fit." The best fit was obtained (to eight significant digits in the squares sum) after a number of cycles roughly equal to one half the number of points in a spectrum. In the later versions of the program, the number of cycles was limited to this value, so as to make more economical use of computer time.

7. Conversion to Center of Mass Coordinates

The conversion to center of mass coordinates has been made by use of the following relations:

$$\text{Let } \gamma^2 = \frac{E}{(E+Q)} \quad \frac{M_1 M_3}{M_2 M_4} \quad \left[\frac{M_3 + M_4}{M_1 + M_2} \right]$$

where $E = \left[M_2/(M_1 + M_2) \right] E_{Lab}$.

$$\text{Then } \theta_{c.m.} = \text{Arcsin}(\theta_{Lab} + \gamma \sin\theta_{Lab}) \qquad \text{(B.11)}$$

$$\text{And } \sigma_{c.m.}(\theta_{cm}) = \sigma_{Lab}(\theta_{Lab}) \left[\frac{\sin\theta_{Lab}}{\sin\theta_{cm}} \right]^3 (1 + \gamma \cos\theta_{cm}) .$$

APPENDIX C

On the Effects of the Electrical Polarizability of the Deuteron on the Elastic Scattering of Deuterons

In connection with stripping calculations, it is of interest to know whether even at bombarding energies such that the plane wave approximation may be justified for the relative motion, the most important effects of distorting forces may not be due to the electrical polarizability of a two-particle system such as the deuteron. This is in fact one of the oldest problems to be considered in deuteron reactions (Oppenheimer 35). More recently, the question of this electrical stretching of the deuteron has cropped up in connection with accurate experiments on the elastic scattering of deuterons (Ford 62, Renken 62).

We shall attempt to calculate the scattering of deuterons by electrostatic forces only, as an example of methods that, with refined techniques, may eventually be applied to scattering and reaction calculations.

The initial assumptions will be that nonrelativistic quantum mechanics is adequate for the problem at hand, that magnetic couplings are small and negligible, and that all the effects of deuteron structure are small enough that a perturbation calculation will suffice.

The zero-order solution is taken to be like the scattering of

two point particles by a Coulomb potential Ze^2/R existing between them. The Hamiltonian of such a system, in coordinates of relative motion, is simply

$$H_o = (-\hbar^2/2M)\ \Delta + Ze^2/R \qquad (C.1)$$

where M is the reduced mass, and R is the magnitude of the separation. Next, we introduce the internal structure of the deuteron. We say that it is composed of two particles, and we denote the proton-neutron Hamiltonian by $H_{np}(\underset{\sim}{r})$, where $\underset{\sim}{r}$ is the position of the proton relative to the center of mass of the deuteron. The next approximation to the total Hamiltonian is then

$$H = H_o + H_{np}(\underset{\sim}{r})\ . \qquad (C.2)$$

This Hamiltonian has eigenfunctions of the form

$$\Psi(\underset{\sim}{R},\underset{\sim}{r}) = \varphi_o(\underset{\sim}{R})\ .\ X_o(\underset{\sim}{r})\ , \qquad (C.3)$$

where $\varphi_o(\underset{\sim}{R})$ is a Coulomb wavefunction with total energy E_o equal to the kinetic energy of the deuteron-nucleus relative motion at large separations, and $X_o(\underset{\sim}{r})$ is the wavefunction of the ground state of the deuteron, having a total energy $E_b = 2.225$ MeV.

The first effect that may be included as a perturbation on the zero-order solutions (C.3) is the correction to the point-charge potential which is necessary because the deuteron is not a point charge but is diffuse. A calculation of this effect has been made by J. B.

French (French 52). In the report of that calculation, an unfortunate choice of terminology has been made, in that the effect has been described as being due to the fact that "...the deuteron is a loose structure with noncoincident centers of mass and charge." This phraseology is incorrect. The diffuseness effect could be present even though the center of mass and center of charge coincide perfectly (as for a hypothetical diproton, for example).

In order to clarify the distinction between the diffuseness effect and the effect of the electrical polarizability, we shall indicate here the procedures for calculating both. This clarification is apparently necessary, because the unfortunate nomenclature of French has been carried over into a comprehensive review paper by Sitenko (Sitenko 59).

The perturbing potential is the difference between the proton-nucleus potential and the potential Ze^2/R, which is written as a deuteron-nucleus potential.

$$V'(\underset{\sim}{R},\underset{\sim}{r}) = Ze^2\left[\frac{1}{|\underset{\sim}{R}-\underset{\sim}{r}|} - \frac{1}{R}\right] . \qquad (C.4)$$

The first term of the perturbing potential may be expanded into a sum of terms proportional to the Legendre polynomials.

No actual analytic calculations may be carried out without further approximations, since we are dealing with a three-body problem. The reduction to two-body problems will be made by assuming

that the adiabatic approximation is valid; that is, the velocities of the proton or neutron relative to their center of mass are much larger than the deuteron velocity, so that a perturbation on the motion of the deuteron as a whole may be computed after first averaging over the proton-neutron positions.

The equation for the wavefunctions of relative motion $\varphi(\underset{\sim}{R})$ is obtained by setting $\Psi(\underset{\sim}{R},\underset{\sim}{r}) = \varphi(\underset{\sim}{R})\ X_o(\underset{\sim}{r})$ into the Schrodinger equation, and integrating over the coordinate $\underset{\sim}{r}$. (We shall indicate this integration by using bra-ket symbols.)

$$H_o\,\varphi(\underset{\sim}{R}) + (X_o|\ V'(\underset{\sim}{R},\underset{\sim}{r})|\ X_o)\,\varphi(\underset{\sim}{R}) = (E - E_b)\,\varphi(\underset{\sim}{R}) \qquad (C.5)$$

Equation (C.5) represents the scattering of a point charge by a diffuse charge distribution having a charge density equal to $X_o^* X_o$. It definitely does not include any effects due to the electrical polarizability. We may see this most directly by explicitly converting the adiabatic perturbing potential $(X_o|\ V'|\ X_o)$ to the classical difference between a point Coulomb potential and the potential due to a charge distribution $\rho(r)$. We do this for the case that X_o is an s-state.

$$V'(\underset{\sim}{R},\underset{\sim}{r}) = Ze^2\left[\sum_n P_n(\cos\theta)\cdot\frac{r_<^n}{r_>^{n+1}} - \frac{1}{R}\right] \qquad (C.6)$$

where $r_<$ is the smaller, and $r_>$ is the larger, of the two radii R and r. When we take the expectation value $(X_o|\ V'|\ X_o)$, only the n = 0 term survives. The answer may be expressed in terms of an

integral having R as a limit of integration, since the n = 0 part of $V'(\underset{\sim}{R},\underset{\sim}{r})$ vanishes when r is smaller than R. If we denote the expectation value as $V'(\underset{\sim}{R})$,

$$V'(R) = \frac{-Ze^2}{R} \int_R^\infty X_o^* X_o + Ze^2 \int_R^\infty X_o^* X_o \frac{1}{r} \quad . \qquad (C.7)$$

This may be explicitly rewritten in a form which has a recognizable meaning in terms of a charge distribution $\rho(r) = X_o^*(r)\, X_o(r)$:

$$V'(R) = \int_o^R \frac{Ze^2}{R} \rho(r) + \int_R^\infty Ze^2 \frac{\rho(r)}{r} - \frac{Ze^2}{R} \qquad (C.8)$$

Potential due to Charge inside R — Potential due to Charge outside R — Point Charge Potential

Thus, the perturbation V'(R) represents an effect due to the diffuseness of the charge distribution of the deuteron, and no allowance has been made as yet for a possible stretching of the deuteron in the electric field of the scattering nucleus.

The existence of an observable effect due to the potential V'(R) is dependent on partial penetration of the scattering nucleus inside the region where the wavefunction of the deuteron $X_o(R)$ is appreciably large. There is then very little hope that small deviations from Rutherford scattering could be unambiguously attributed to the diffuseness of the deuteron rather than to an effect of the nuclear forces. The potential V'(R) vanishes with increasing R in a way governed by the way

in which $X_o(\underset{\sim}{r})$ vanishes with increasing r, which is exponential. This will contrast with the results of the perturbation due to the electrical polarizability, which has an asymptotic behavior proportional to $1/R^4$.

We may consider the effect of the polarizability in the adiabatic approximation as follows. We set $\Psi(\underset{\sim}{R},\underset{\sim}{r}) = \varphi(\underset{\sim}{R})\, X(\underset{\sim}{r},\underset{\sim}{R})$ into the Schrodinger equation. If we neglect velocities $\dot{\underset{\sim}{R}}$ compared to $\dot{\underset{\sim}{r}}$, we obtain an equation for $X(\underset{\sim}{R},\underset{\sim}{r})$ with an eigenvalue depending on R

$$H_{np}X(\underset{\sim}{R},\underset{\sim}{r})+V'(\underset{\sim}{R},\underset{\sim}{r})\, X(\underset{\sim}{R},\underset{\sim}{r}) = E_b(\underset{\sim}{R})\, X(\underset{\sim}{R},\underset{\sim}{r}) \,. \qquad (C.9)$$

If we use the eigenvalue $E_b(R)$ instead of E_b in the equation

$$H_o\varphi(\underset{\sim}{R}) + E_b(\underset{\sim}{R})\, \varphi(R) = E\varphi(R) \qquad (C.9a)$$

we will obtain a description of the scattering which includes both the effect of the diffuseness and that of the induced polarization of the deuteron.

In order to obtain analytic estimates, we shall need to make simplifications in the problem just stated. In the region outside the nuclear charge distribution, $V'(R,r)$ is given by the expansion (C.6). Let us suppose further that we are sufficiently far outside, that there is very little overlap of the deuteron charge distribution with the nuclear charge distribution. With typical nuclear dimensions, this may be said to happen when the deuteron-nucleus separation is larger than 7 or 8 Fm. The typical deuteron dimension is near 2 Fm. In

order to obtain good solutions $X(\underset{\sim}{R},\underset{\sim}{r})$ from equation (C.9), we need to use an expression for $V'(\underset{\sim}{R},\underset{\sim}{r})$ which is good in a region centered about the tip of $\underset{\sim}{R}$, and having dimensions of 2 or 3 Fm. The expression (C.6) in this region is an expansion in a power series of a parameter which is always smaller than say, 3/7. Thus it makes good sense to keep only the leading terms, for example,

$$V'(\underset{\sim}{R},\underset{\sim}{r}) = \frac{Ze^2}{R}\left[\left(\frac{r}{R}\right)\cos\theta + \left(\frac{r}{R}\right)^2 P_2(\cos\theta) + \ldots\right] \qquad (C.10)$$

Only the first of these two terms can produce a stretching of the deuteron so as to displace the center of mass from the center of charge. Thus, the effects of the dipole polarizability may be estimated by simply considering the deformation of the deuteron by a constant field, having a linear potential $(Ze^2/R^2)r\cos\theta$.

The largest term in the interaction is that due to the dipole moment induced in the deuteron. We assume that this dipole moment is simply proportional to the electric field $\underset{\sim}{E}$,

$$\underset{\sim}{P} = a\,\underset{\sim}{E}\,.$$

The interaction energy is then

$$(1/2)\,\underset{\sim}{P}\cdot\underset{\sim}{E} = (a/2)\,\underset{\sim}{E}\cdot\underset{\sim}{E} = (a/2)\,(Ze/R^2)^2\,. \qquad (C.11)$$

This is the perturbing potential we wish to consider, at least when R is sufficiently large.

Such a potential is highly singular at R = 0, and yields infinite matrix elements for the perturbation if it is continued to R = 0. It is therefore imperative to consider what happens as the deuteron approaches the scattering center. The value which is obtained in any estimate of the deuteron polarizability shows that the average displacement of the proton from the deuteron center of mass is very small compared to the deuteron radius for electric fields of the magnitudes encountered in nuclear problems. Thus the induced dipole continues to be the leading term at all separations R. As a guide in considering what shape may be ascribed to this term of the interaction, we consider the interaction of a point dipole with a diffuse central charge distribution. We have

$$V''(R) = (a/2)\, E^2$$
$$E = (Ze/R^2) \int_0^R 4\pi\, \rho(r)\, r^2\, dr\,. \qquad \text{(C.12)}$$

In the special case that $\rho(r)$ is constant inside a sphere of radius R_o, the electric field is

$$\begin{aligned} E &= ZeR/R_o^3 && R < R_o \\ E &= Ze/R^2 && R > R_o \end{aligned} \qquad \text{(C.13)}$$

The interaction potential of this charge distribution is then

$$\begin{aligned} V''(R) &= (a/2)(Ze)^2\, R^2/R_o^6\,, && R < R_o \\ V''(R) &= (a/2)(Ze)^2\, /R^4\,, && R > R_o\,. \end{aligned} \qquad \text{(C.14)}$$

If the charge distribution has a diffuse surface, the electric field has no sharp peak at $R = R_o$. A potential which reduces to (C.14) except in the vicinity of the nuclear surface, where it has the qualitative properties of a potential corresponding to a diffuse surface, is the following

$$V''(R) = (a/2)(Ze)^2 \; R^2/ (R^6 + b^6) . \qquad (C.15)$$

The parameter b determines the average radius. We may obtain some understanding of the nature of this assumption by deducing what charge distribution would indeed lead to (C.15). This is plotted in Figure 17. The form (C.15) has been chosen so as to allow a particularly simple evaluation of some integrals we shall need to do later.

A convenient way to estimate the effects of the potentials $V'(R)$, due to the diffuseness, and $V''(R)$, due to the polarizability, on the elastic scattering, is to use the Born approximation. This method has the advantage of giving analytic answers which allow a more accessible understanding of the angle and energy dependence. For very low bombarding energies, the Born answer is likely to be too large. For example, the calculations of French (French 52) show that the answer obtained by using Coulomb waves appropriate to a point charge, rather than plane waves, gives an answer six times smaller than the Born answer for the scattering of 14 MeV deuterons by aluminium. This is a calculation of the effect of diffuseness. The

effects of V''(R) are likely to be less wrong, as calculated by the Born approximation, because the Born approximation is most inaccurate near R = 0. For the diffuseness effect, the perturbation is largest near R = 0, whereas for the effect of the polarizability, the chosen potential (C.15) is zero at R = 0. It should also be noted that the use of Coulomb wavefunctions may give an answer which is too small for either effect, since the electrical potential due to the scattering nucleus is actually expected to remain finite rather than diverge like a point charge potential as $R \to 0$.

For spherically symmetric potentials, the matrix element in Born approximation is given by

$$V_{fi} = 4\pi \int_0^\infty V(r) \frac{\sin qr}{qr} r^2 \, dr \qquad \text{(C.16)}$$

where q is the momentum transfer, $\underset{\sim}{q} = \underset{\sim}{k}_f - \underset{\sim}{k}_i$ in terms of the wave vectors $\underset{\sim}{k}_f$ and $\underset{\sim}{k}_i$ of the final and initial relative motion. For the potential due to the polarizability (C.15), this integral may be conveniently done by extending the domain of integration to $-\infty$, and replacing sin qr by $e^{iqr}/2i$. A straightforward computation of the residues yields for the matrix element

$$V''_{fi} = (a/2)\, 4\pi\, (Ze)^2 \frac{1}{q} \frac{1}{b^2} \Big[e^{-qb/2} \cos[\, qb\sqrt{(3/4)} - \pi/3] - e^{-qb}\, 2/3 \Big] \qquad \text{(C.18)}$$

In order to obtain the fractional deviation from pure Rutherford scattering, we must add this amplitude to the scattering amplitude corresponding to the unperturbed potential. As is well known, the first Born approximation gives the correct answer,

$$(Ze^2/r)_{fi} = 4\pi\ Ze^2/q^2 \quad . \tag{C.19}$$

Since we know that the plane wave is a poor approximation to the zero-order wavefunction, especially for low bombarding energies, we may consider modifications in our procedure to take account of some known effects. We might for example consider the direct use of Coulomb wavefunctions having asymptotically a definite wave vector; the matrix element of V''(R) would be

$$(V'')_{fi} = \int \frac{e^{iq.r}}{q}\ F(in_1,\ 1,\ -ik.r + ikr)\ F(in_2,\ 1,\ -ik'.r + ik'r)$$
$$V''(r)\ r^2\ dr\ d\Omega \quad . \tag{C.20}$$

In this expression, n_1 and n_2 are the Coulomb parameters of the initial and final relative motion. The evaluation of this integral has been attempted by Y. N. Kim (Kim 61) for $V''(r) \propto 1/r^4$. The graph shown in this paper as the fractional deviation from Rutherford of the cross section has a damped oscillatory character with increasing angle, as does our result (C. 18), and it gives deviations of the same magnitude. A more detailed comparison is not possible because there is no explicit

mention of how the divergence of $1/r^4$ at the origin was circumvented.

In order to estimate whether the plane-wave approximation gives the correct magnitude even if the wavefunctions are not correctly given near $r = 0$, we may consider modifying our estimate (C.16) by use of a penetration factor. We know that the wavefunction in the $L = 0$ channel should be most strongly modified. Thus, we know that it is oscillatory for distances larger than the classical turning point, and that it damps out exponentially towards the origin from the turning point. We modify the potential $V''(r)$ so that the $L = 0$ part is more nearly right, by multiplying it by a factor which is 1 at large distances and is smaller near the origin. The partial waves of higher L are less affected by the penetration factor. A particularly simple evaluation of the matrix element is possible in our case if we choose a penetration factor of the form $G(r) = r^2/(r^2 + d^2)$, where d is a length of the order of the classical turning point for $L = 0$. The integration is easily carried out by summing residues as we did in obtaining (C.18). The result is

$$V''_{fi} = (a/2)4\pi(Ze)^2 \frac{1}{q}\left[e^{-qb/2} \frac{d^2\cos[qb\sqrt{(3/4)}] + b^2\cos[qb\sqrt{(3/4)} - \pi/3]}{d^4 + b^4 + 2b^2d^2\cos(\pi/3)}\right.$$

$$\left. + \frac{e^{-qb}}{2d^2(1 - b^2/d^2)} + \frac{e^{-qd}}{2d^2(b^6/d^6 - 1)}\right] . \qquad \text{(C.21)}$$

The formulae (C.18) or (C.21) enable us to give a numerical estimate of the effects of polarizability as soon as we have calculated

the deuteron polarizability a and made some justification for the use of the point-dipole approximation.

A convenient quantum-mechanical estimate of the polarizability may be obtained if the neutron-proton interaction is of the harmonic oscillator type. In this case, we may solve for the deuteron wavefunction X(r) keeping both terms of the perturbation V'(R,r) as given by (C.10), without great difficulty. The first term simply translates the origin of the paraboloid representing the potential, and the second term changes slightly the frequency of oscillation; the change in frequency is negligible in our estimate. In terms of the proton mass and the frequency in the radial direction, the displacement of the center of the proton potential is

$$d = eE(R)/mw^2 \qquad (C.22)$$

The induced dipole moment is simply ed, so that the polarizability is

$$a = e^2/mw^2 \ . \qquad (C.23)$$

The point dipole approximation will be justified if we can show that for values of w^2 appropriate to the deuteron, the induced displacement of the proton is always small compared to the coordinate of the deuteron center of mass.

The values of w^2 appropriate for the deuteron may be estimated in various ways. For example, we know that the ground state of the

deuteron is bound by 2 MeV by a potential of depth near 38 MeV (Fowler 60); this suggests that we set $\hbar w = 24$ MeV. Another estimate may be made from the known size of the deuteron; the decay length s of a harmonic-oscillator wavefunction is related to w^2 by $mw^2 = \hbar^2/ms^4$, and we know that 1/e decay length of the deuteron is of the order of 2 Fm. These and other (Kim 61) estimates of the deuteron polarizability suggest that we should use a value near

$$a \cong 0.09 \text{ fermi}^3 . \qquad (C.24)$$

With this value, we find that the stretching of the deuteron due to nuclear electric fields will be rather small. The maximum electric fields are to be found at the nuclear surface. If we assume a nuclear radius $R_n = R_o A^{1/3}$, with $R_o = 1.2$ Fm, the maximum fields corresponding to a uniform charge distribution inside the nuclear volume produce a displacement

$$d = a E / e = a Z /(R_o^2 A^{2/3}) = 0.0625 Z A^{-2/3} \text{ fermi} .$$

This is a small fraction of the typical deuteron dimension near 2 Fm for all nuclei. For ^{208}Pb, it amounts to 8 percent, and this may well be an overestimate, since the maximum electric fields for a charge distribution having a diffuse edge will be even smaller.

The fractional deviation from Rutherford scattering due to the stretching of the deuteron is to be estimated by adding the perturbation amplitudes (C.18) or (C.21) to (C.19) and squaring, and comparing

the result to the pure Rutherford scattering, which is the square of (C.19). At bombarding energies of a few MeV or less on light nuclei, the deviations are never larger than a few percent. For example, it is 2 percent for deuterons elastically scattered from lithium at a bombarding energy of 1 MeV at 180°.

The smallness of this result suggests that effects of deuteron stretching are generally negligible. At bombarding energies such that they might be appreciable, thereis strong probability of interference from nuclear scattering. In addition, there is a possibility that magnetic or relativistic effects might also be important. It will not be possible to disentangle these small effects until relativistic equations are developed which are appropriate to describe the motion of the deuteron.

REFERENCES

(Ajzenberg-Selove 59) F. Ajzenberg-Selove and T. Lauritsen, Nuclear Physics 11, 1 (1959).

(Bardin 61) R. K. Bardin, Thesis, California Institute of Technology (unpublished).

(Beckner 61) E. H. Beckner, C. M. Jones, and G. C. Phillips, Phys. Rev. 123, 255 (1961).

(Birks 61) J. B. Birks (editor), Proceedings of the Rutherford Jubilee International Conference, Heywood, London, 1961.

(Butler 57) S. T. Butler and O. Hittmair, Deuteron Stripping Reactions, Wiley, New York, 1957.

(Dietrich 60) F. S. Dietrich and L. Cranberg, Bull. Am. Phys. Soc. 5, 493 (1960).

(El Nadi 61) M. El Nadi and H. Sherif, Nuclear Physics 28, 331 (1961).

(Elton 62) L. R. Elton and Daphne F. Jackson, Nuclear Physics 35, 209 (1961).

(Erskine 61) J. R. Erskine and C. P. Browne, Phys. Rev. 123, 958 (1961).

(Ford 62) J. L. C. Ford, Thesis, California Institute of Technology (unpublished).

(Fowler 47) W. A. Fowler, C. C. Lauritsen, and T. Lauritsen, Rev. Sci. Inst. 18, 818 (1947).

(Fowler 58) W. A. Fowler, Course Notes for Nuclear Physics 203, California Institute of Technology (unpublished).

(French 52) J. B. French and M. L. Goldberger, Phys. Rev. 87, 899 (1952).

(Gibbs 61) W. R. Gibbs, Thesis, Rice Institute, Houston, 1961 (unpublished). Some of this material has been published in W. Tobocman and W. R. Gibbs, Phys. Rev. 126, 1076 (1962).

(Jarmie 61) N. Jarmie, M. G. Silbert, and D. B. Smith, Nuclear Physics 25, 443 (1960).

(Kim 61) Y. N. Kim, Nuovo Cimento 22, 885 (1961).

(Landau 57) L. D. Landau, Lectures on Nuclear Theory, Consultants Bureau, Inc., New York, 1957.

(Li 51) C. W. Li, Thesis, California Institute of Technology (unpublished).

(Marion 60) J. B. Marion, 1960 Nuclear Data Tables, part 3, U. S. Atomic Energy Commission, 1960.

(Messiah 61) A. Messiah, Mecanique Quantique, Dunod, Paris, 1961.

(Newns 60) H. C. Newns, Proc. Roy. Soc. 76, 489 (1960).

(Nordberg 61) M. E. Nordberg, Thesis, California Institute of Technology (unpublished).

(Nordberg 62) M. E. Nordberg, F. B. Morinigo, and C. A. Barnes, Phys. Rev. 125, 321 (1962).

(Oppenheimer 35) J. R. Oppenheimer and M. Phillips, Phys. Rev. 48, 500 (1935).

(Overley 61) J. C. Overley, Thesis, California Institute of Technology (unpublished).

(Phillips 60) G. C. Phillips, T. A. Griffy, and L. C. Biedenharn, Nuclear Physics 21, 327 (1960).

(Renken 62) J. Renken, private communication, 1962.

(Saxon 61) R. S. Saxon, in discussions at the Direct Interactions Sessions of the Rutherford Jubilee International Conference (Birks 61).

(Schiff 55) L. I. Schiff, Quantum Mechanics, McGraw Hill, 1955.

(Sitenko 59) A. G. Sitenko, Soviet Physics Uspekhi 67, 195 (1959).

(Shapiro 61) I. S. Shapiro, Nuclear Physics 28, 244 (1961).

(Slattery 57) J. C. Slattery, R. A. Chapman, and T. W. Bonner, Phys. Rev. 108, 809 (1957).

(Tobocman 61) W. Tobocman, Theory of Direct Nuclear Reactions, Oxford University Press, 1961.

(Whaling 58) W. Whaling, The Energy Loss of Charged Particles in Matter, in Encyclpedia of Physics, vol. 34, S. Flügge, 1958.

(Whaling 60) W. Whaling, in Nuclear Spectroscopy, Ed. by F. Ajzenberg-Selove, Academic Press, 1960.

(Wilkinson 58) D. H. Wilkinson, Phil. Mag. 3, 1185 (1958).

TABLE I

Spectrometer Calibration Constant

The calibration constant of the magnetic spectrometer k_m as determined relative to the electrostatic analyzer during the course of the experiment, using widely different values of the spectrometer angle and magnet current. The definition of k_m is given in Appendix B, Section 1. The deviations from the average have been taken as an indication of the overall absolute errors to be expected from the energy scale of the analyzer and spectrometer. Textual references, pp. 25, 73.

TABLE I

Spectrometer Calibration Constants

Oct 10, 1960	0.3988
Oct 12, 1960	0.4004
Jan 5, 1961	0.4005
Jan 8, 1961	0.4006
Jan 12, 1961	0.3984
Feb 18, 1961	0.3951
May 7, 1961	0.3983
May 31, 1961	0.4057
June 2, 1961	0.4063
June 4, 1961	0.4050
Aug 14, 1961	0.4004
Aug 16, 1961	0.3983

Average and Variance = 0.4003 ± 0.0037

Fractional Variance = 0.009

TABLE II

Solid Angle and Resolution of Spectrometer

The instrumental constant of the spectrometer, as measured by elastically scattering the incident beam on the thick target backings. We quote the ratio of the measured value to the nominal constant obtained from the previously accepted values of the parameters, the Rutherford cross section, and the published stopping cross sections, as is explained in Appendix B, Section 3. The deviations from 1 are an indication of the absolute precision with which the cross sections are being measured with our equipment, for a case in which the number of target nuclei is well known.

Textual references, pp. 26, 76.

TABLE II

Solid Angle and Resolution of Spectrometer

A	1.11
B	0.94
C	0.97
D	1.10
E	0.92
F	1.03
G	0.91
H	0.88
I	1.04

Average and Variance = 0.99 ± 0.08

Fractional Variance = 0.08

TABLE III

Averages of Q Values and Widths

Summary of the averages of Q values and level widths, as determined from the best fits found by the computer program described in Appendix B, Section 6. In computing these averages, we have rejected those spectra which were recorded under known adverse conditions of target contamination and stability. The standard deviations quoted are $1/\sqrt{(n-1)}$ times the variance of the n values used in computing the average. The errors quoted represent a quadratic combination of fractional uncertainties, including the standard deviation, the uncertainty in the energy calibration, and an uncertainty ascribed to possible surface contaminations. For comparison, we also show the results of Erskine and Browne (Erskine 61).

Textual references, pp. 29.

TABLE III

Averages of Q Values and Widths

Quantity		Value		Error	Standard Deviation
Q_a	=	0.156	±	0.006 MeV	0.005 MeV
Q_b	=	-0.154	±	0.008 MeV	0.006 MeV
$Width_a$	=	0.082	±	0.006 MeV	0.004 MeV
$Width_b$	=	0.093	±	0.007 MeV	0.005 MeV

Values from Erskine and Browne (Erskine 61)

Q_a	=	0.163	±	0.010 MeV	
Q_b	=	-0.143	±	0.010 MeV	
$Width_a$	=	0.085	±	0.020 MeV	
$Width_b$	=	0.095	±	0.020 MeV	

TABLE IV

Differential Cross Sections for $Li^6(He^3, p)Be^{8*}$

Differential cross sections (in millibarns) for the reactions A: $Li^6(He^3, p)Be^{8*}(16.63)$ and B: $Li^6(He^3, p)Be^{8*}(16.94)$. The values are the result of a fit of the data, whose details are given in Appendix B. All energies are in MeV. The errors assigned to the points are relative within each energy; they have been estimated from the statistical errors of the measurements, and the uncertainties in target normalization, and the general quality of the fit. The fractional absolute errors are of the order of 20 percent. This estimate is the result of a quadratic combination of the uncertainties in the instrumental calibration (Table II), in the target thickness measurements (Figure 7), and in the purity of the lithium layer.

Textual references, p. 34.

TABLE IV

Differential Cross Sections for $Li^6(He^3, p)Be^{8*}$

Center of Mass Energy	$Angle_A$	$Cross\ Section_A$	$Angle_B$	$Cross\ Section_B$
1.178	55	5.47 ± 0.65	56	3.31 ± 0.55
1.184	104	2.64 ± 0.45	106	1.70 ± 0.31
1.177	145	1.15 ± 0.45	146	0.92 ± 0.50
1.404	0	2.25 ± 0.35	0	0.60 ± 0.17
1.407	19	2.59 ± 0.40	19	0.75 ± 0.18
1.396	37	2.18 ± 0.31	37	0.68 ± 0.19
1.393	55	1.13 ± 0.22	56	0.96 ± 0.18
1.403	72	1.11 ± 0.19	73	0.47 ± 0.14
1.416	88	0.98 ± 0.18	90	0.44 ± 0.13
1.430	104	0.61 ± 0.16	105	0.42 ± 0.12
1.412	37	4.22 ± 0.68	38	2.36 ± 0.28
1.429	55	3.70 ± 0.55	56	2.01 ± 0.35
1.440	72	3.47 ± 0.52	73	1.75 ± 0.34
1.433	88	2.06 ± 0.45	90	1.03 ± 0.31
1.443	104	2.31 ± 0.46	105	0.98 ± 0.30
1.458	118	1.81 ± 0.35	120	0.88 ± 0.25
1.450	132	1.70 ± 0.30	133	0.89 ± 0.32
1.445	145	1.84 ± 0.31	146	0.65 ± 0.29
1.427	157	0.70 ± 0.29	158	

TABLE IV (continued)

Center of Mass Energy	$Angle_A$	$Cross\ Section_A$	$Angle_B$	$Cross\ Section_B$
1.550	0	3.80 ± 0.62	0	1.46 ± 0.32
1.546	19	3.26 ± 0.72	19	1.28 ± 0.36
1.553	37	3.70 ± 0.64	38	0.92 ± 0.38
1.518	55	3.05 ± 0.48	56	2.73 ± 0.50
1.532	72	2.50 ± 0.42	73	1.37 ± 0.38
1.547	88	1.90 ± 0.36	90	1.24 ± 0.28
1.566	104	1.55 ± 0.34	105	0.90 ± 0.31
1.669	0	10.71 ± 1.60	0	3.10 ± 0.89
1.661	19	12.72 ± 1.90	0	2.99 ± 0.81
1.660	37	9.22 ± 1.20	38	3.93 ± 0.72
1.654	55	8.78 ± 1.20	56	2.41 ± 0.65
1.672	72	7.20 ± 0.85	73	2.82 ± 0.60
1.687	88	6.32 ± 0.66	90	2.69 ± 0.55
1.692	104	6.74 ± 0.86	105	2.22 ± 0.58
1.690	118	4.64 ± 0.84	120	2.59 ± 0.54
1.695	132	3.57 ± 0.78	133	2.07 ± 0.60
1.694	145	3.37 ± 0.74	146	1.19 ± 0.65
1.696	157	3.26 ± 0.70	158	0.89 ± 0.52

TABLE V

Total Cross Sections for $Li^6(He^3, p)Be^{8*}$

Total cross sections (in millibarns) for the reactions A: $Li^6(He^3, p)Be^{8*}$ (16.63) and B: $Li^6(He^3, p)Be^{8*}$ (16.94). All energies are in MeV. These values have been obtained by integrating the differential cross sections as given by the theoretical fits to the measured values given in Table IV. The errors assigned represent an absolute error estimated from the uncertainties in the fit, and the absolute accuracy of the measurements of the target thickness and of the instrumental constant. For completeness, we include the total cross sections at two higher energies, calculated directly from the measured cross sections of Erskine and Browne (Erskine 61).

Textual references, pp. 36.

TABLE V

Total Cross Sections for $Li^6(He^3,p)Be^{8*}$

Laboratory Energy	Center of Mass Energy	Cross Section A	Cross Section B
1.8	1.18	42 ± 12	22 ± 7
2.2	1.41	35 ± 13	15 ± 8
2.4	1.55	25 ± 8	12 ± 4
2.6	1.68	75 ± 27	20 ± 11
3.5	2.30	58 ± 25[a]	38 ± 19[a]
4.25	2.80	45 ± 23[a]	33 ± 15[a]

[a]Computed from results of Erskine and Browne (Erskine 61)

FIGURE 1

The Energy Levels of Be^8

The present experiment has investigated the levels at excitations between 14 and 17 MeV. No trace was found of the level indicated at 16.08 MeV. One of the two levels at 16.63 and 16.94 MeV is expected to be the T = 1 analog of the ground states of Li^8 and B^8, which have $J = 2^+$. The other level is expected to be T = 0, since apparently it has no analog in Li^8 or B^8. The results tend to favor the identification of the 16.63 level as having T = 1 and $J = 2^+$. The most straightforward interpretation of the data suggests that the 16.94 level has $J = 4^+$.

Textual references, pp. 1, 12, 13.

FIGURE I

THE ENERGY LEVELS OF Be^8

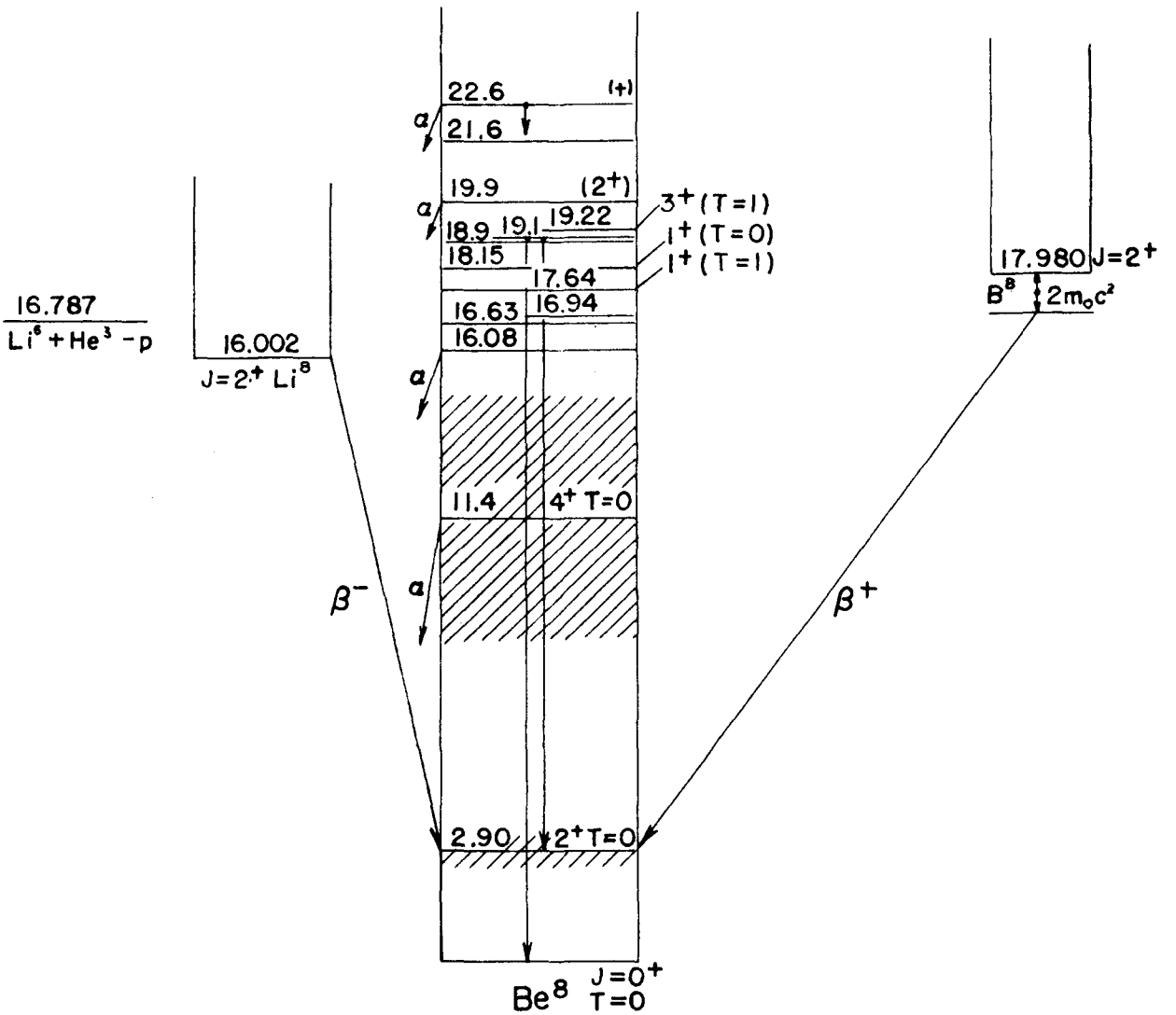

FIGURE 2

A Typical Proton Spectrum from the Spectrometer

In this figure one may see a plot of the raw data as obtained in the spectrometer, in the form of a number of proton counts at various fluxmeter volts I. The proton energy is given in MeV approximately by $E_p = 0.4/I^2$. In this particular spectrum, taken at 45° in the laboratory at a bombarding energy near 2 MeV, one sees clearly resolved the peaks corresponding to excitation energies of 16.63 and 16.94 MeV in Be^8. An arrow at the left indicates roughly the position to be expected for protons leaving Be^8 at 16.08 MeV excitation. No bump at this excitation energy showed up in any spectrum. An arrow at the right indicates roughly the position to be expected for protons leaving Be^8 at an excitation of 17.64 MeV. The state at this excitation was never resolved from the background due to protons of 1/3 the machine energy scattered elastically from the thick target backing; it was only seen as a small knee in the elastic proton step, which begins near 0.75 volts in this particular spectrum.

Textual references, pp. 5, 6, 33.

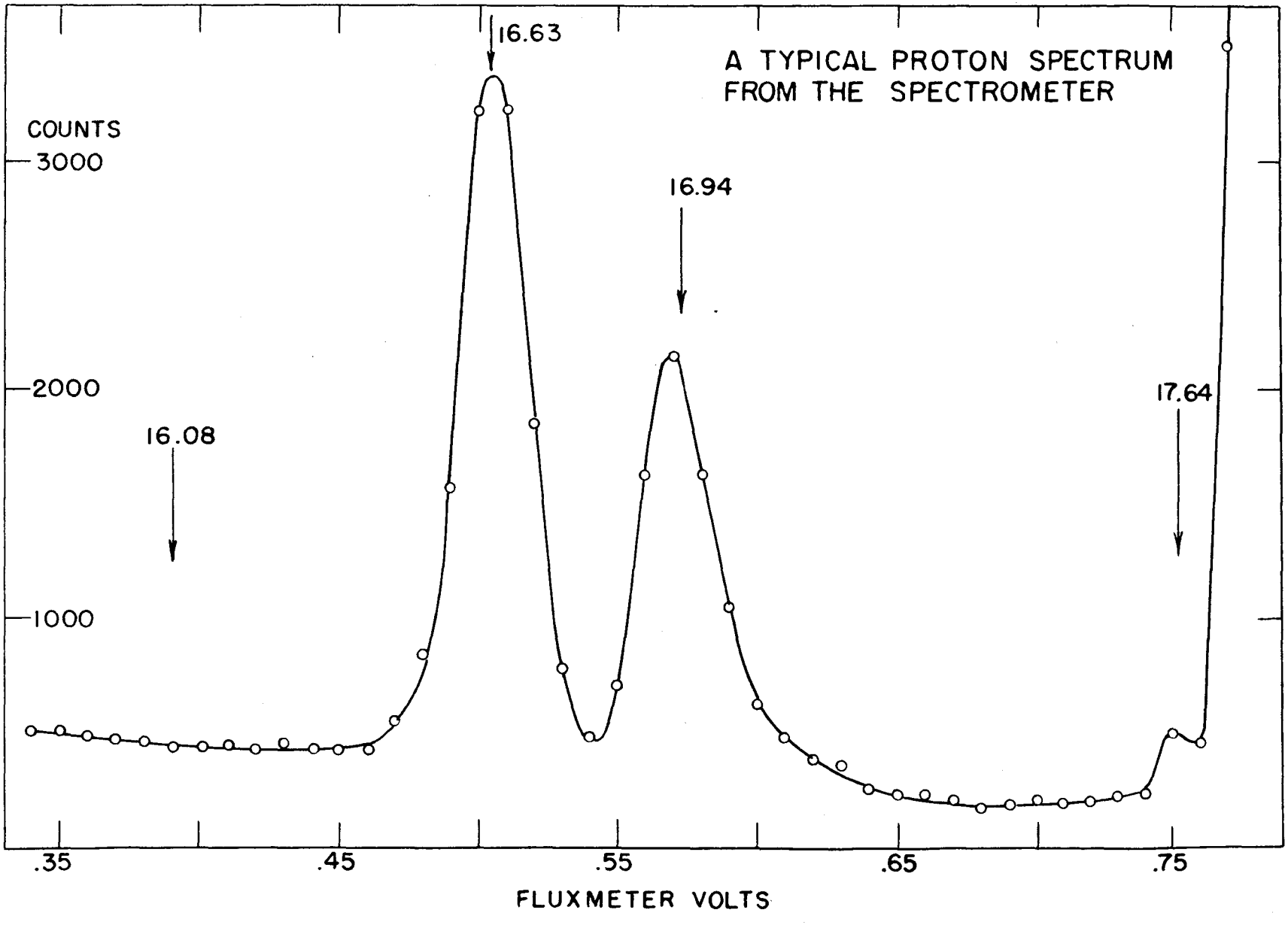
A TYPICAL PROTON SPECTRUM
FROM THE SPECTROMETER
16.63
16.94
16.08
17.64
COUNTS
3000
2000
1000
.35
.45
.55
.65
.75
FLUXMETER VOLTS

FIGURE 2

FIGURE 3

A Typical Alpha-Particle Spectrum from the Spectrometer

We show here the raw data, in the form of alpha counts versus fluxmeter setting, of the alpha-spectrum observed at 150° in the laboratory upon bombardment of Li^6 by He^3 particles of 2.6 MeV energy. The chief feature is a plateau-like structure which has been interpreted in terms of the breakup of the two excited levels of Be^8 at 16.63 and 16.94 MeV. The edges of the plateau are indicated by arrows, together with the corresponding alpha energy. Spectra such as these were corrected for energy losses in the target and converted to a velocity spectrum in order to compare them with the kinematic predictions (Figure 5).

Textual references, pp. 6, 30, 13.

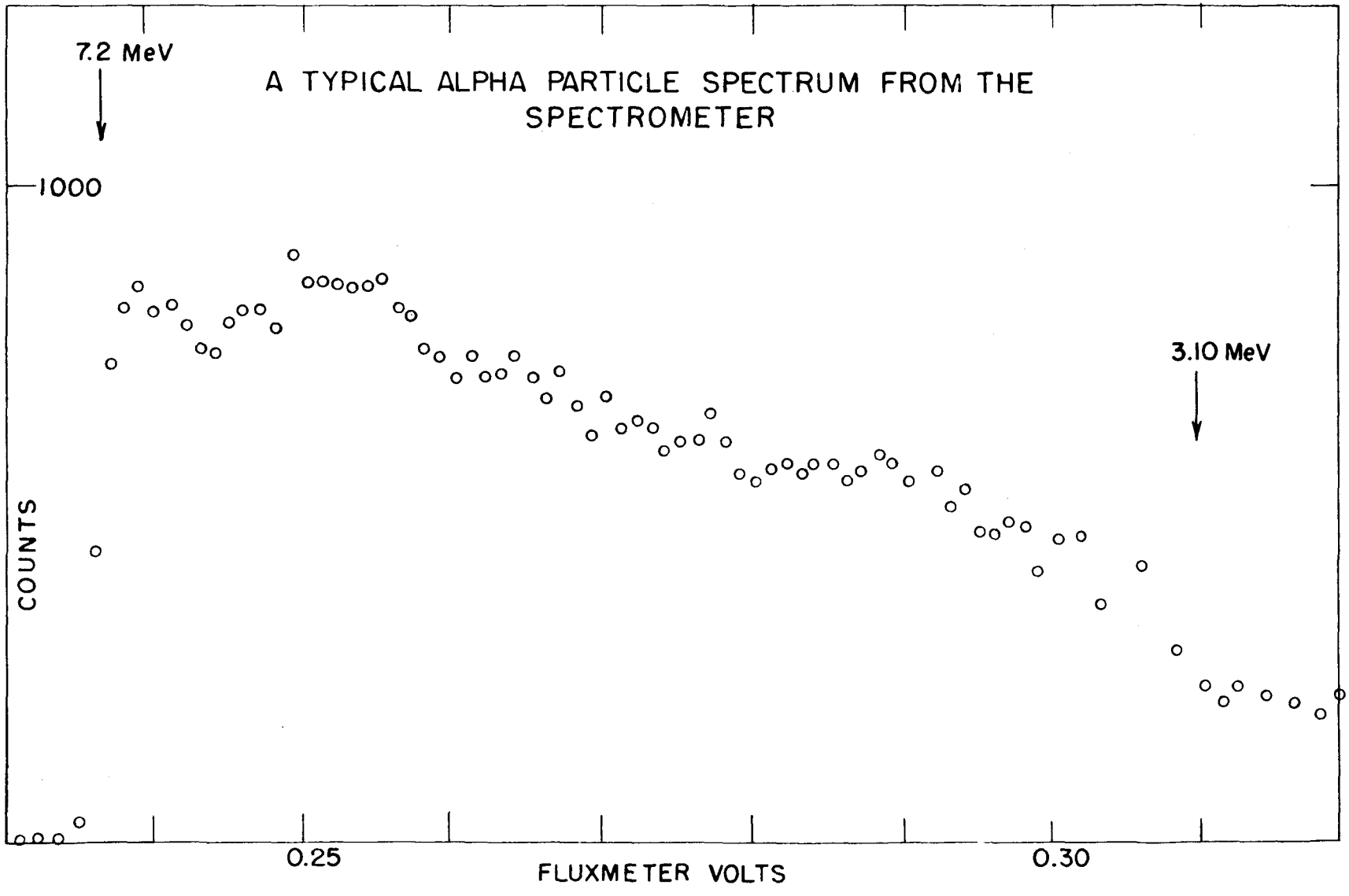
7.2 MeV
A TYPICAL ALPHA PARTICLE SPECTRUM FROM THE SPECTROMETER
1000
3.10 MeV
COUNTS
0.25
FLUXMETER VOLTS
0.30

FIGURE 3

FIGURE 4

Pulse Height Spectrum for a Thin Counter

This is a typical pulse height spectrum for a thin counter in the target chamber. The counts above channel 30 are attributed to alpha particles, since the maximum pulse height for protons was approximately at channel 30. The structure between channels 45 and 75 corresponds to an alpha-plateau similar to that of Figure 3. The energy scale is approximately linear with channel number, and the counter resolution is approximately 4 channels for alpha particles of 6 MeV, which appear at channel 55.

Textual references, pp. 14, 16, 29.

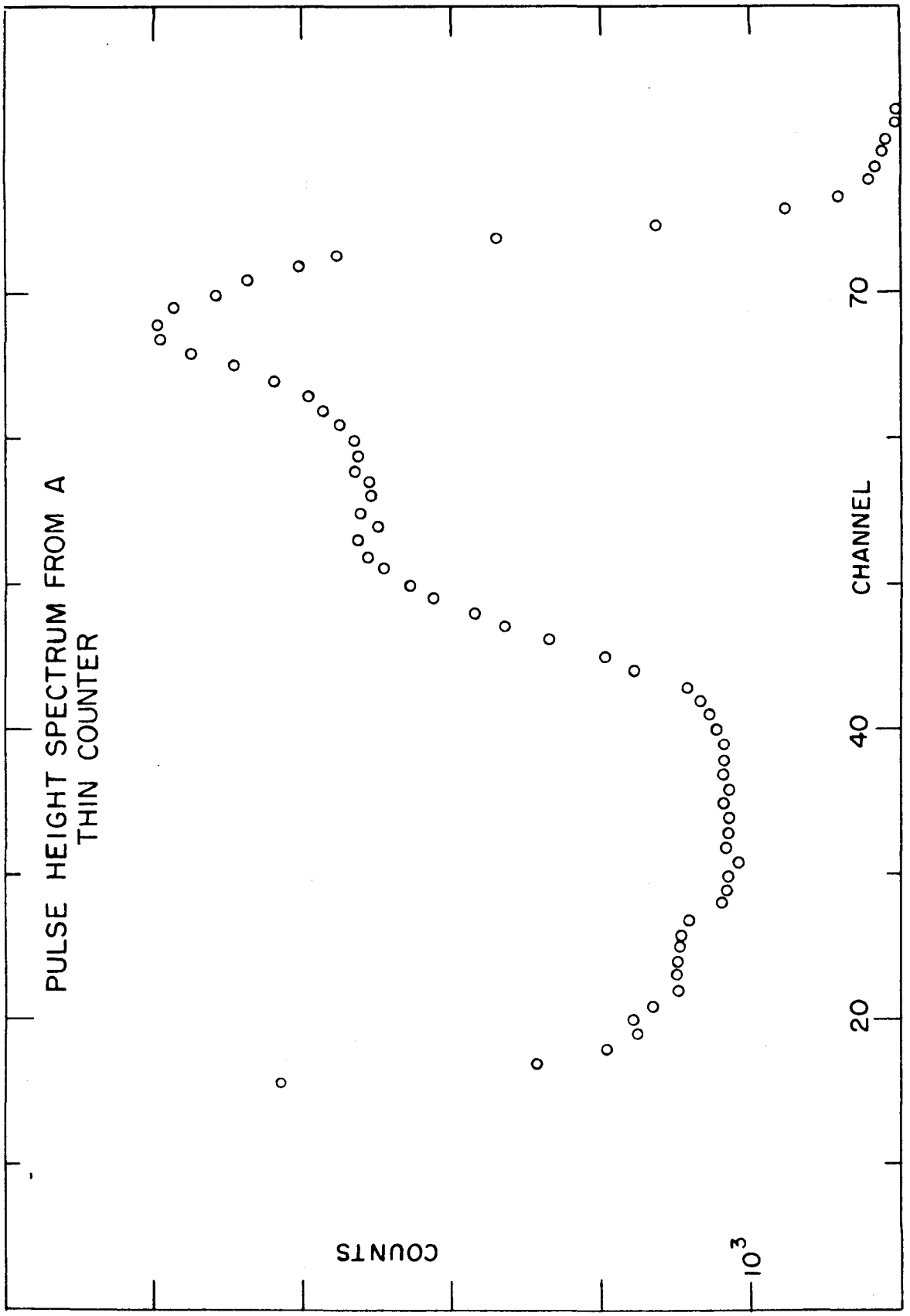
PULSE HEIGHT SPECTRUM FROM A
THIN COUNTER
COUNTS
10^3
CHANNEL
20
40
70

FIGURE 4

FIGURE 5

Target Profiles

These are typical of the data used to compute the spectrometer calibration and the target thicknesses. The solid dots represent the profile of protons of 1.2 MeV energy, scattered elastically on a bare tungsten backing. The open circles represent the profile of protons after the evaporation of a lithium layer on the surface of the tungsten. The solid lines are smooth curves drawn through the points to aid in locating the midpoint of the rise of the profiles. The steepness of the rise of the second profile is an indication of the homogeneity of the lithium layer over an area of the size of the beam spot.

Textual references, pp. 10, 12, 24, 35, 73.

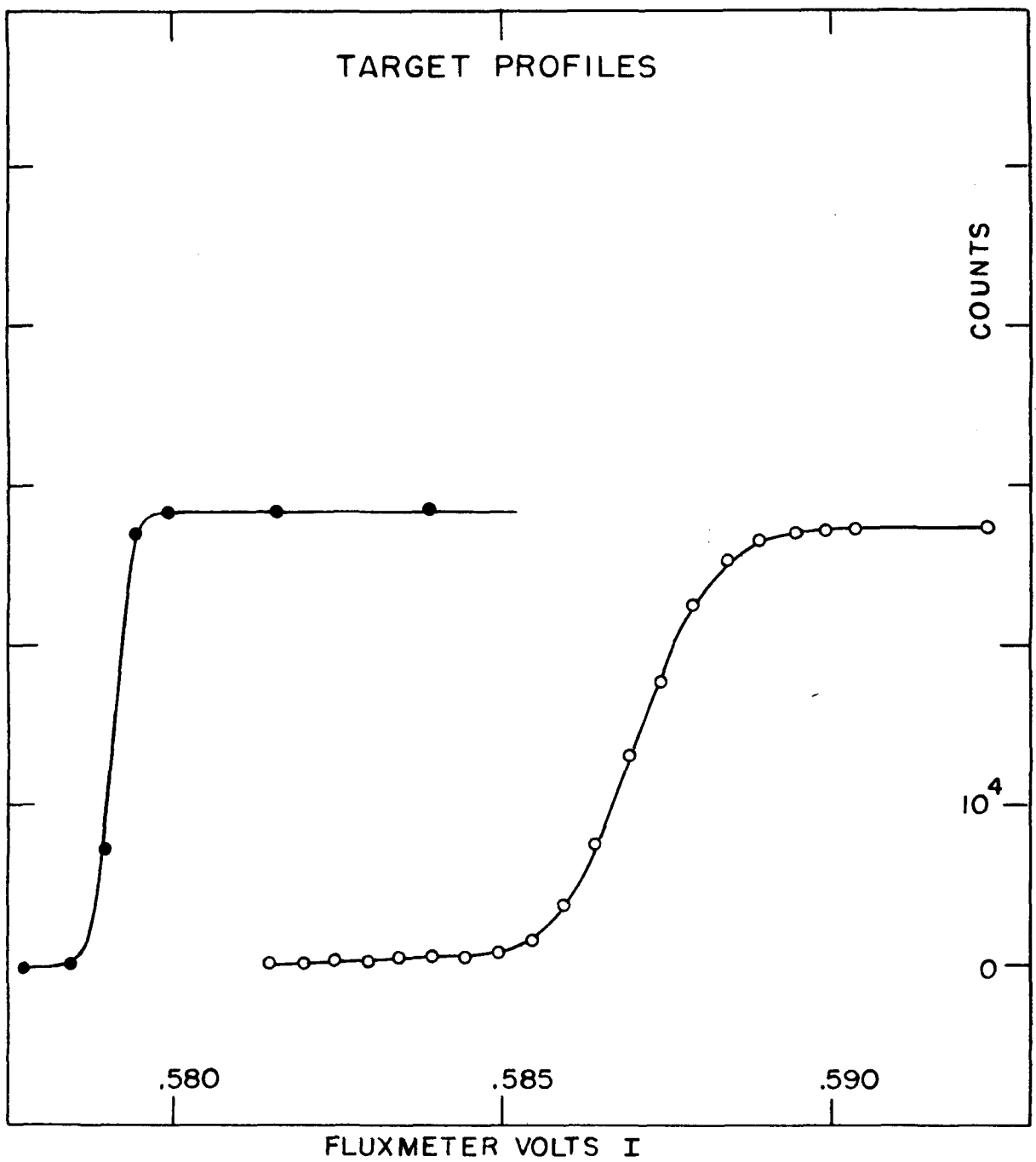

FIGURE 5

FIGURE 6

A Good Q Value Spectrum

This spectrum is typical of the ones obtained in the runs to determine Q values and level widths. The vertical scale is millibarns per steradian MeV. The horizontal scale shows the Q value in MeV. The points have been obtained from raw data such as are shown in Figure 2 by the computer program, which converted the raw data as is discussed in Appendix B, Section 6. The solid curve is the result of a fit with a function which is the sum of a constant background plus two bumps of the Breit-Wigner shape. The differential cross section corresponding to this bombarding energy has been calculated from the parameters of the fit, as is discussed in Appendix B, by multiplying the height times the half width times the factor $\pi/2$.

Textual references, pp. 34.

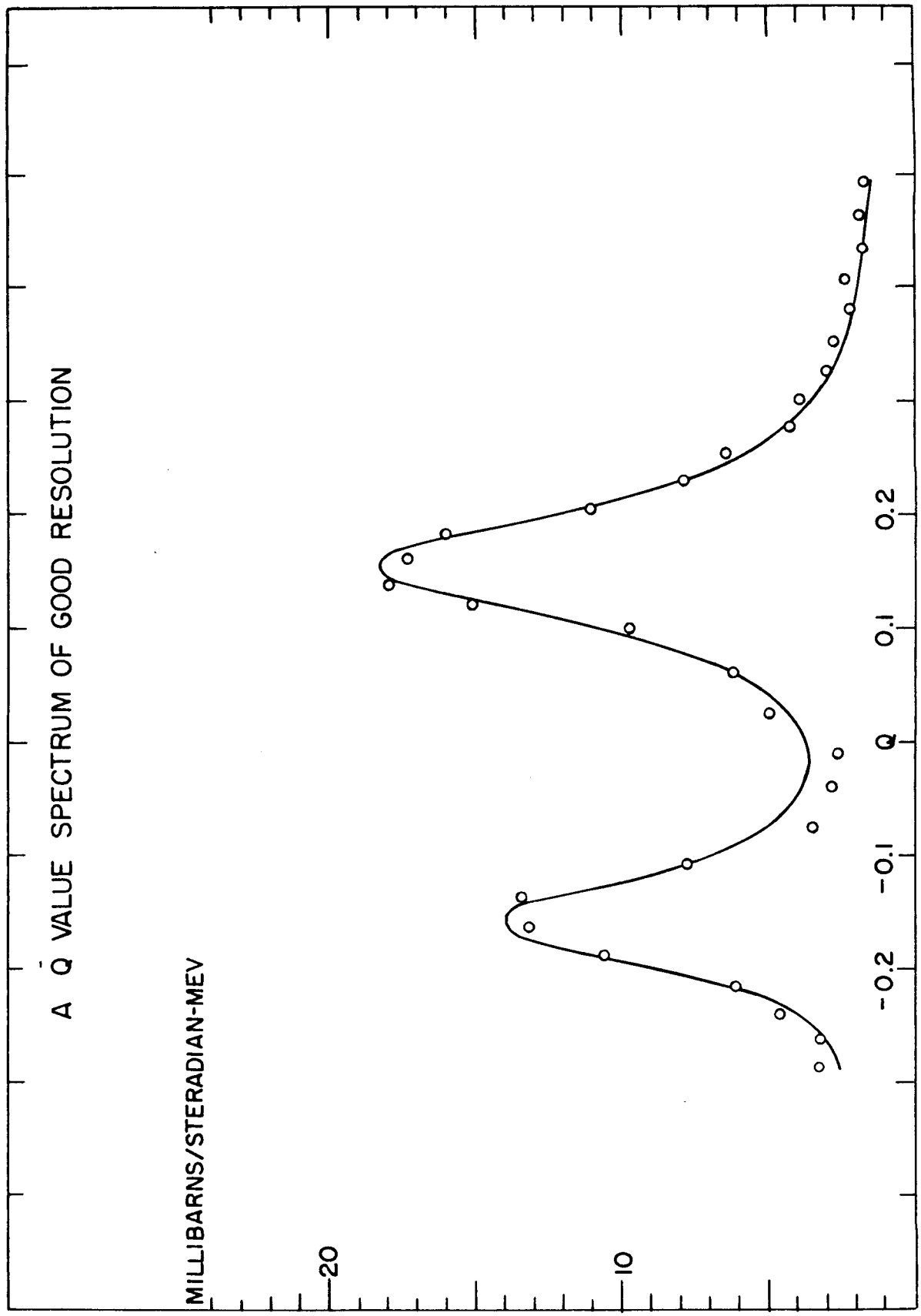
A Q̄ VALUE SPECTRUM OF GOOD RESOLUTION
MILLIBARNS/STERADIAN-MEV
20
10
0.2
0.1
Q
-0.1
-0.2

FIGURE 6

FIGURE 7

Velocity Spectrum of Alpha Particles

This is the velocity spectrum of alpha particles produced by bombarding Li^6 by He^3 of 2.2 MeV energy, observed at 90° in the laboratory. The horizontal scale is in units of c, where c is the velocity of light. The curves shown represent the spectra to be expected from the decay of one infinitely sharp level in Be^8 at an excitation energy of 16.787 MeV. One dotted line corresponds to an isotropic distribution of the protons in the Li^6 (He^3, p) reaction. The solid line corresponds to a forward-peaked distribution of the protons, of the form $(1 + a \cos\theta)$, with $a = 0.26$. A second dotted line corresponding to $a = 0.5$ has been drawn to illustrate the sensitivity of the theoretical shape to the degree of forward peaking, as described by the parameter a. The points have been obtained from spectrometer measurements of the type illustrated in Figure 3. The calculations of the idealized spectra have been made by using equations (A.20) and (A.21) of Appendix A.

Textual references, pp. 30, 31, 71, 73.

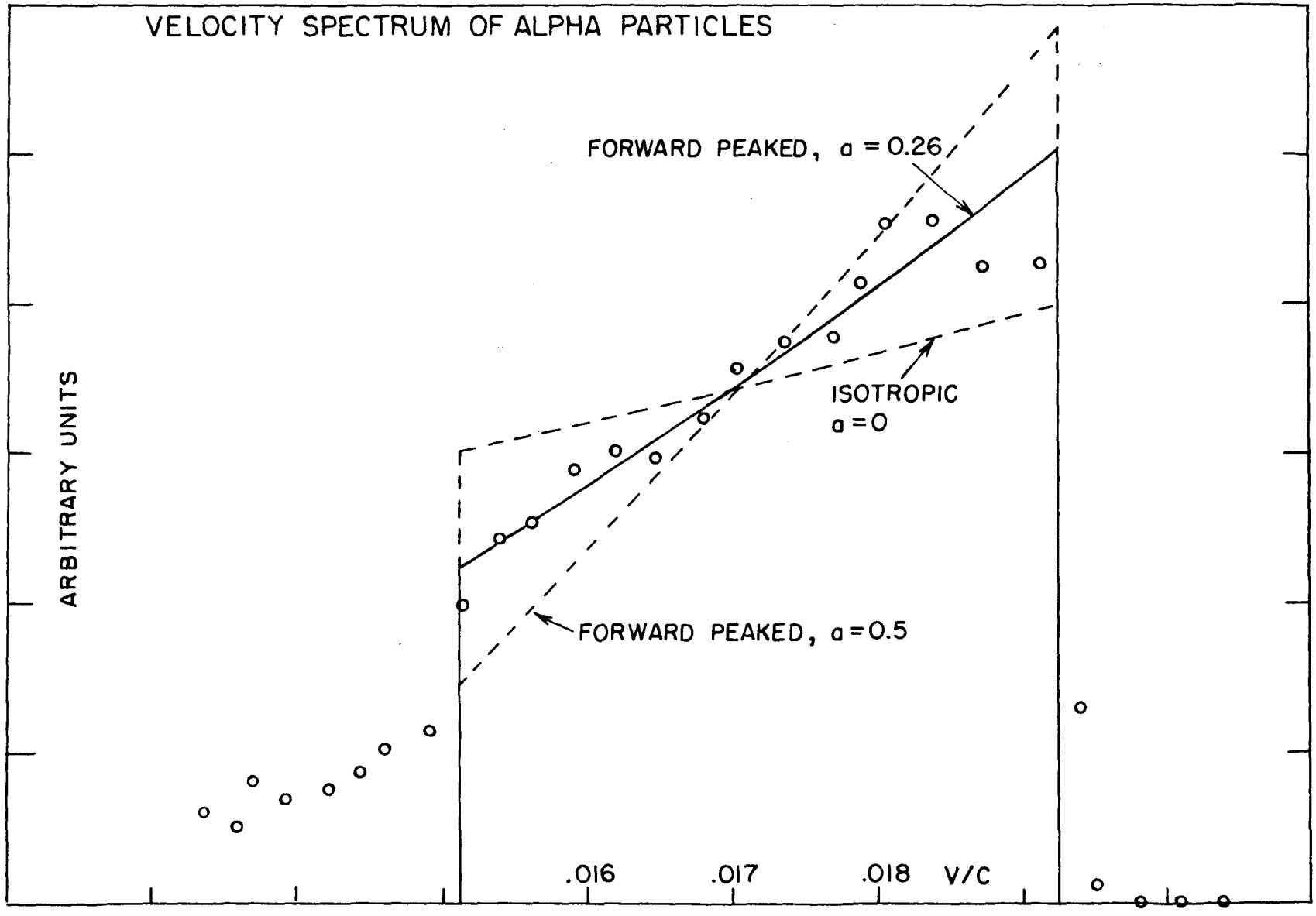
VELOCITY SPECTRUM OF ALPHA PARTICLES
FORWARD PEAKED, a = 0.26
ISOTROPIC
a = 0
FORWARD PEAKED, a = 0.5
ARBITRARY UNITS
.016
.017
.018
V/C

FIGURE 7

FIGURE 8

Alpha Particles in Coincidence with Protons

We show a pulse height spectrum of alpha particles in coincidence with protons corresponding to an excitation of 16.63 MeV in Be^8. The angular positions of the counter and spectrometer were such that the lower edge of the plateau was expected to be in coincidence. The shape of the ungated pulse height spectrum is shown as a dotted line. A smooth curve of a shape generally compatible with the counter resolution for alpha particles has been drawn to guide the eye. A discussion of this measurement is to be found in Part II, Section 3.

Textual references, pp. 6, 16, 32.

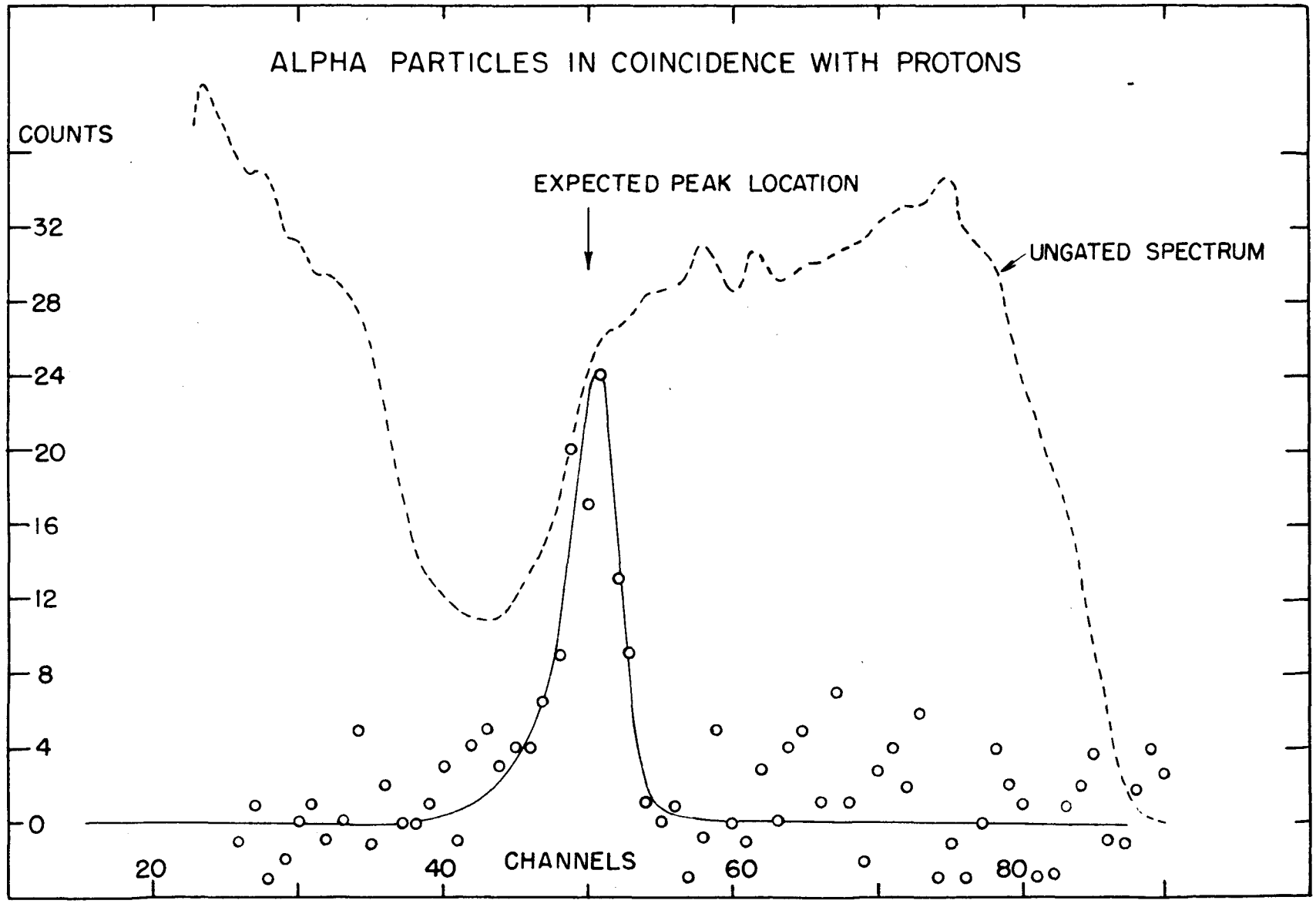
ALPHA PARTICLES IN COINCIDENCE WITH PROTONS
COUNTS
EXPECTED PEAK LOCATION
UNGATED SPECTRUM
32
28
24
20
16
12
8
4
0
20
40
CHANNELS
60
80

FIGURE 8

FIGURE 9

A Q Value Spectrum from an Oxidized Target

This spectrum is typical of those considered to have given a relatively unreliable value for the differential cross sections. This is a transmission spectrum, observed at 2.2 MeV bombarding energy at 0° in the laboratory. The target had been evaporated on an aluminium foil of 0.8 mils thickness. The lithium layer had been allowed to oxidize at a small pressure of air in an attempt to prevent diffusion of the metallic lithium into the aluminium backing. The smooth curve represents the fit obtained by the computer program described in Appendix B. The experimental procedures from which such spectra were obtained are discussed in Part II, Section 2.

Textual references, pp. 34.

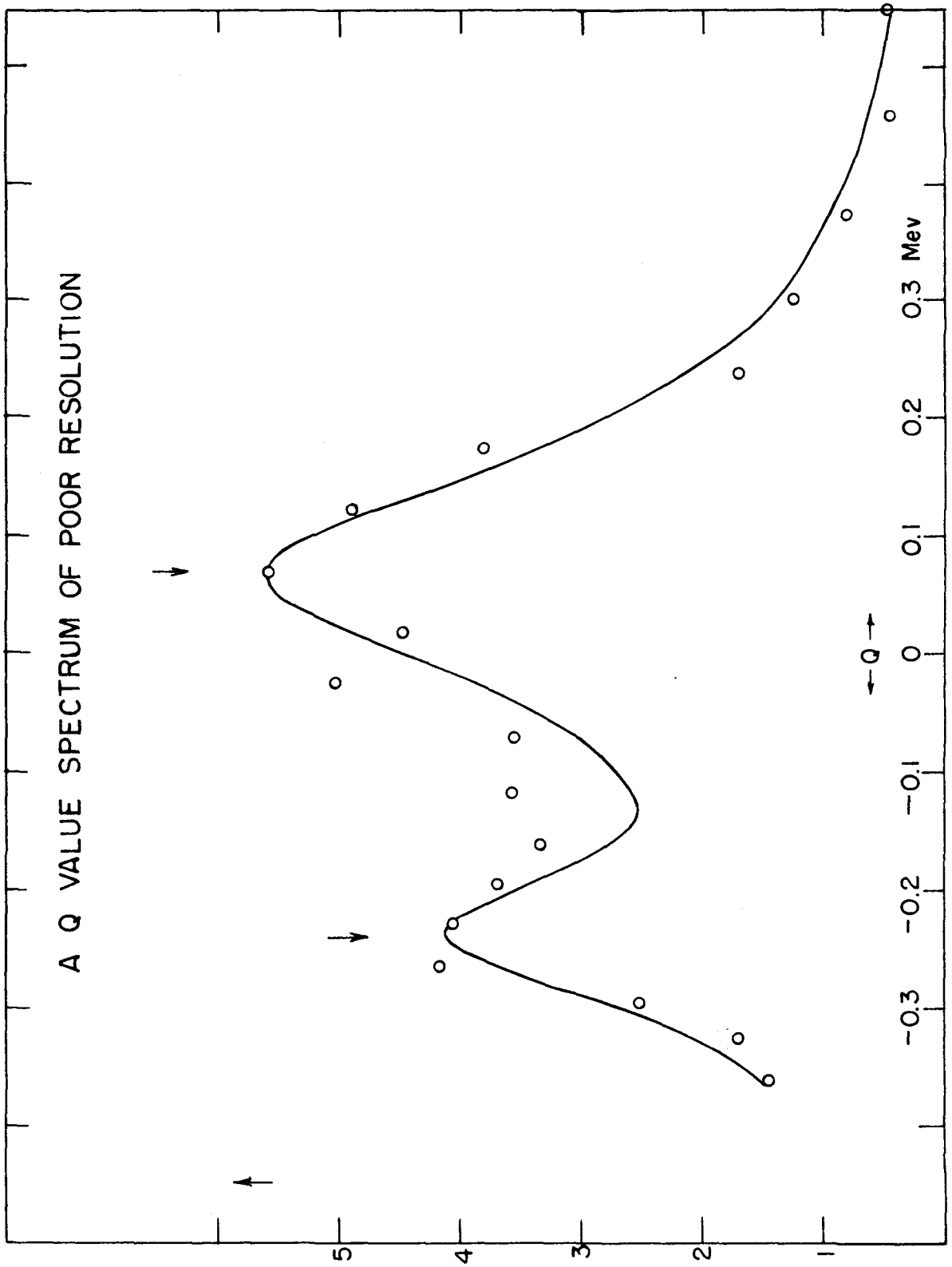
A Q VALUE SPECTRUM OF POOR RESOLUTION
0.3 Mev
0.2
0.1
0
-0.1
-0.2
-0.3
-Q
5
4
3
2
1

FIGURE 9

FIGURE 10

Differential Cross Sections at 1.18 MeV

This is a plot of the differential cross sections in the center of mass system, from measurements made at energies near 1.8 MeV in the laboratory (Table IV) using a thick copper backing. The error bars represent the best estimate of the relative uncertainties. The absolute uncertainty of the values on the scale at the left is estimated to be 20 percent. The smooth curves represent the theoretical fits obtained using the simplest plane-wave theory described in Part IV; the algebraic form and the parameters are given in Part V.

Textual references, pp. 5, 36, 60, 61.

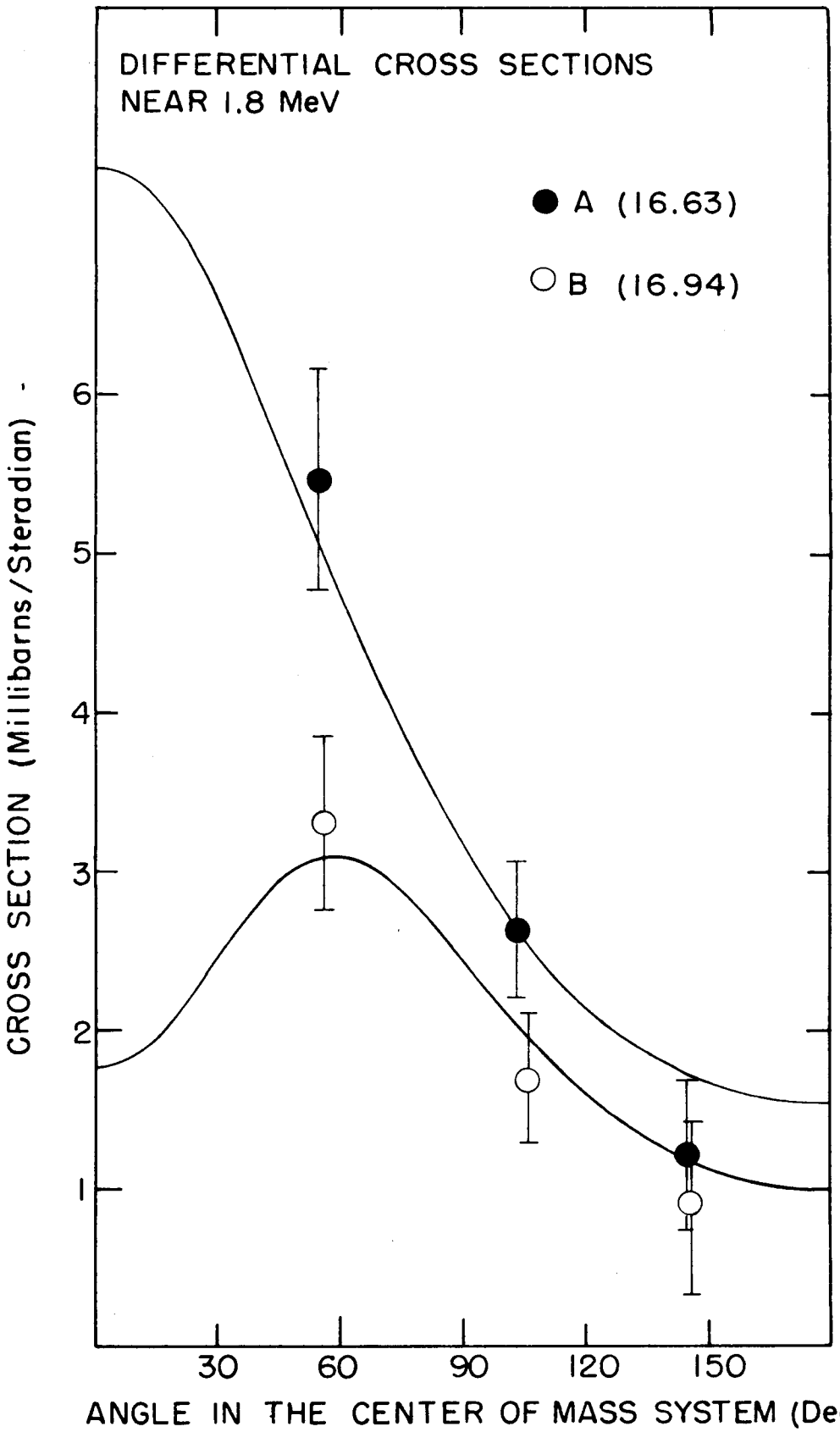
DIFFERENTIAL CROSS SECTIONS
NEAR 1.8 MeV
A (16.63)
B (16.94)
CROSS SECTION (Millibarns/Steradian)
1
2
3
4
5
6
30
60
90
120
150
ANGLE IN THE CENTER OF MASS SYSTEM (Deg)

FIGURE 10

FIGURE 11

Differential Cross Sections at 1.41 MeV (foil backing)

This is a plot of the differential cross sections in the center of mass system, from the measurements at energies near 2.2 MeV in the laboratory (Table IV). The error bars represent relative uncertainties. The absolute uncertainty in the scale at the left is estimated to be 20 percent. With this estimated uncertainty, the magnitudes of this group of measurements are not in good agreement with those shown on Figure 12. Since these points represent measurements made on a target which had been allowed to oxidize, the discrepancy in magnitude may be attributed to an incorrect assignment of lithium content in this target. The angular distribution should be unaffected by this error. The solid curves represent fits with formulae from the theory discussed in Part IV; the algebraic form and the parameters are discussed in Part V.

Textual references, pp. 36, 60, 61.

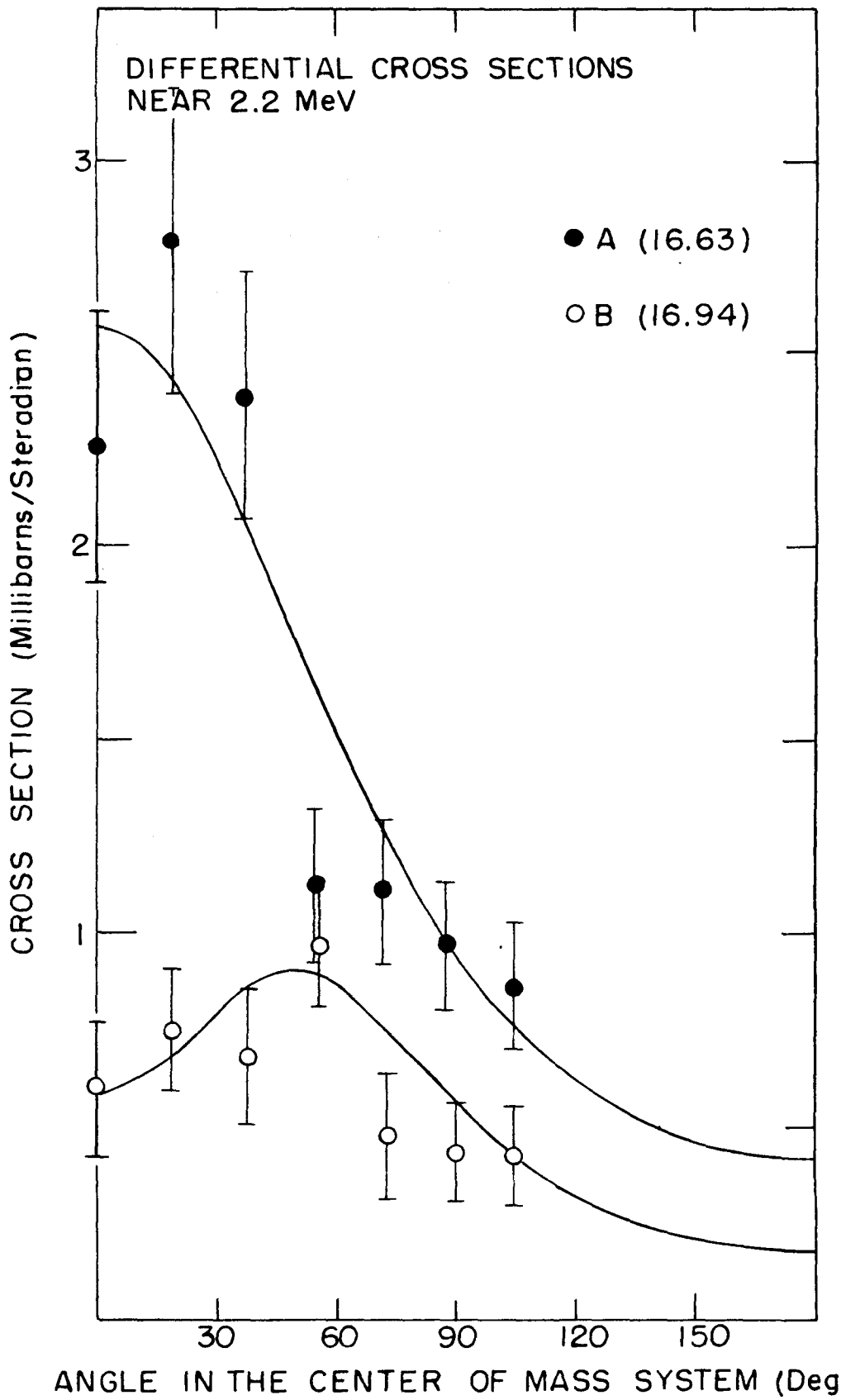
DIFFERENTIAL CROSS SECTIONS
NEAR 2.2 MeV
A (16.63)
B (16.94)
CROSS SECTION (Millibarns/Steradian)
3
2
1
30
60
90
120
150
ANGLE IN THE CENTER OF MASS SYSTEM (Deg)

FIGURE 11

FIGURE 12

Differential Cross Sections at 1.42 MeV (thick backing)

This is a plot of the differential cross sections in the center of mass system, from the measurements made at energies near 2.2 MeV in the laboratory (Table IV) using a thick tungsten backing. The error bars represent relative uncertainties. The absolute uncertainty in the scale at the left is estimated to be 20 percent. The absolute magnitudes of cross sections such as these, obtained from thick-backing targets, are expected to be somewhat more reliable than those obtained on thin-backing targets. The smooth curves represent fits made with the formulae from the theory developed in Part IV and discussed in Part V.

Textual references, pp. 36, 60, 61.

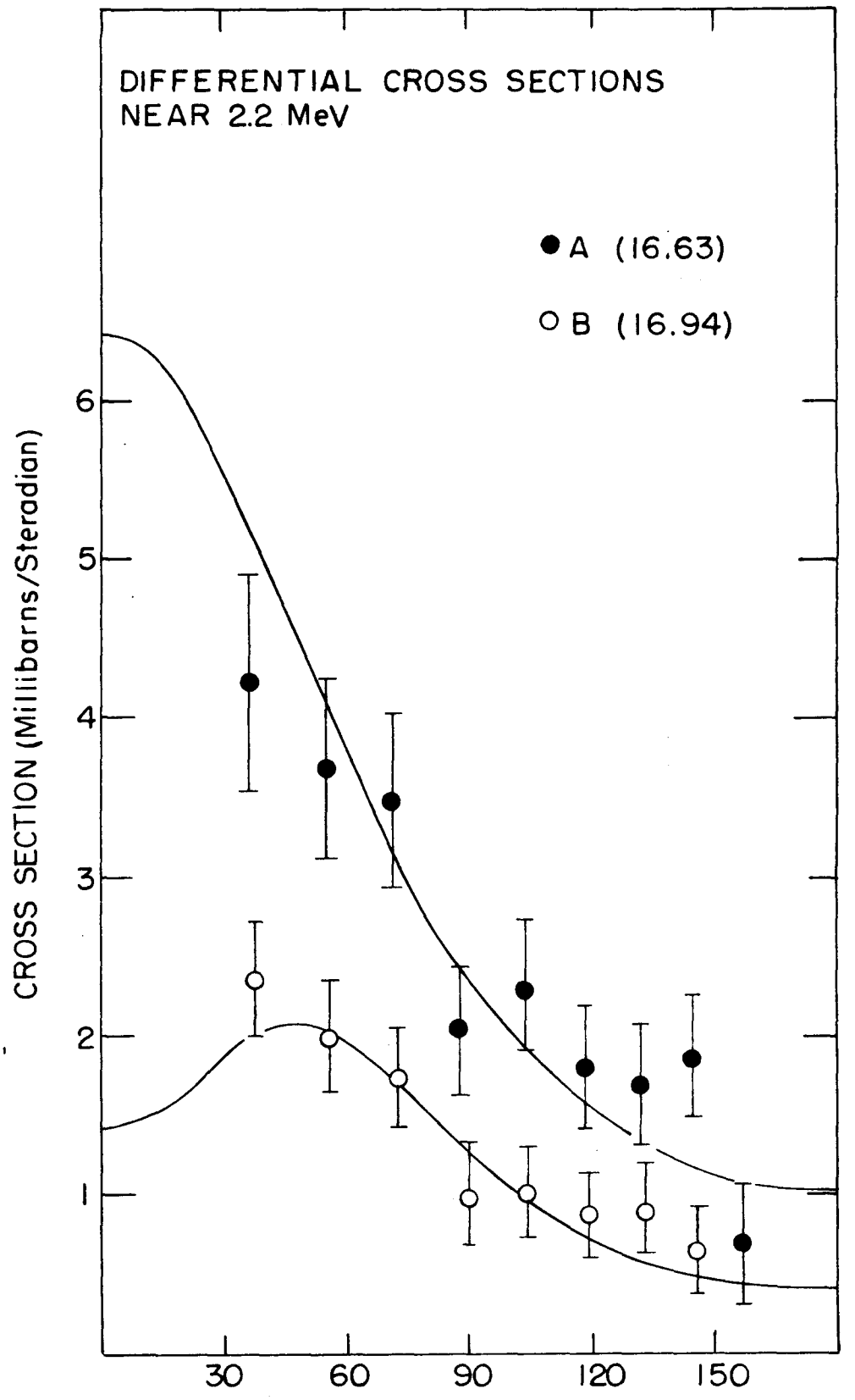
DIFFERENTIAL CROSS SECTIONS
NEAR 2.2 MeV
● A (16.63)
○ B (16.94)
CROSS SECTION (Millibarns/Steradian)
1
2
3
4
5
6
30
60
90
120
150
ANGLE IN THE CENTER OF MASS SYSTEM (Deg)

FIGURE 12

FIGURE 13

Differential Cross Sections at 1.55 MeV

This is a plot of the differential cross sections in the center of mass system, from data obtained at a bombarding energy of 2.4 MeV in the laboratory. The error bars represent relative uncertainties. The absolute uncertainties in the scale at the left are estimated to be 20 percent. The smooth curves represent fits using the theory developed in Part IV, and discussed in Part V. These measurements were made on the same aluminium foil backing. The measurements plotted in Figure 12 represent data obtained with a thick tungsten backing.

Textual references, pp. 36, 60, 61.

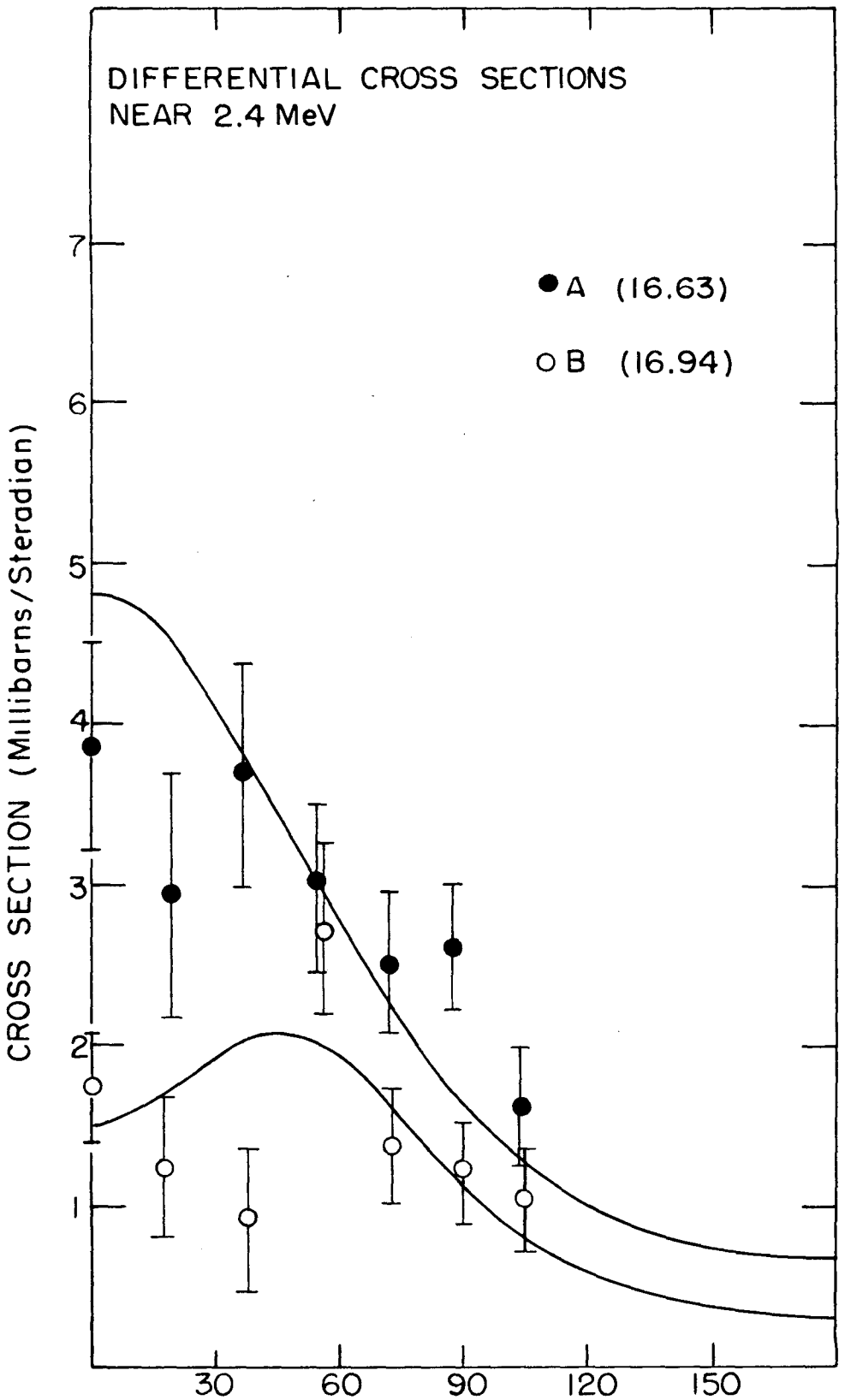
DIFFERENTIAL CROSS SECTIONS
NEAR 2.4 MeV
● A (16.63)
○ B (16.94)
CROSS SECTION (Millibarns/Steradian)
7
6
5
4
3
2
1
30
60
90
120
150
ANGLE IN THE CENTER OF MASS SYSTEM (Deg.)

FIGURE 13

FIGURE 14

Differential Cross Sections at 1.66 MeV

This is a plot of the differential cross sections in the center of mass system, from the measurements made at energies near 2.6 MeV in the laboratory (Table IV). The error bars represent relative uncertainties. The absolute uncertainties in the vertical scale at the left are estimated to be 20 percent. The solid curves represent fits using the theory developed in Part IV and discussed in Part V. The triangular points represent data obtained from a target evaporated on a foil. The round points represent data obtained from a target evaporated on a thick tungsten backing. Thus, consistent results from different target backings are available between 90 and 30 degrees at this bombarding energy.

Textual references, pp. 36, 60, 61.

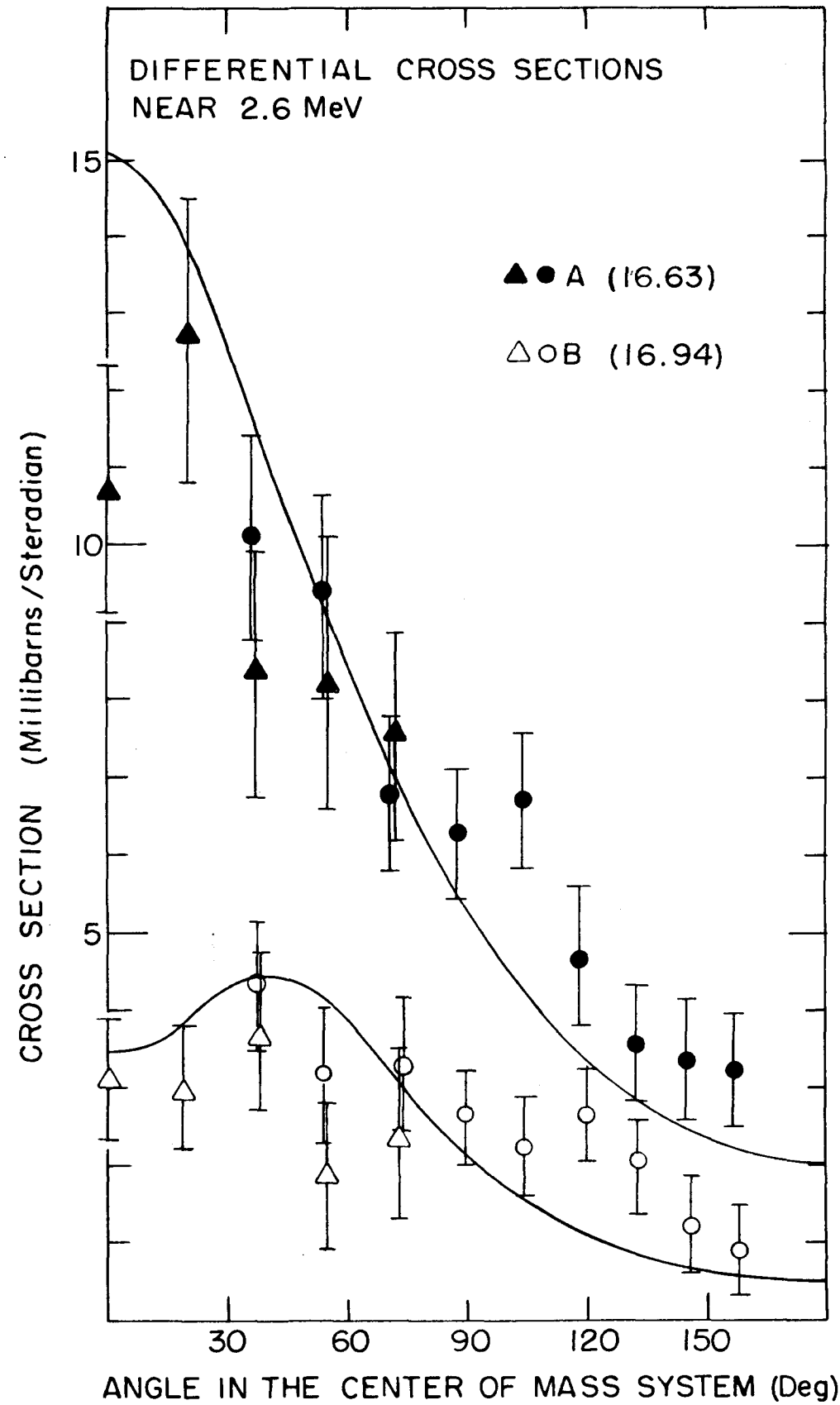
DIFFERENTIAL CROSS SECTIONS
NEAR 2.6 MeV
▲● A (16.63)
△○B (16.94)
CROSS SECTION (Millibarns/Steradian)
15
10
5
30
60
90
120
150
ANGLE IN THE CENTER OF MASS SYSTEM (Deg)

FIGURE 14

FIGURE 15

The Identification of Clusters in Direct Reactions

The labels A, B, and C correspond to the formulae in the discussions of direct reactions, in Part IV. We show the identification of the clusters for some of the possible reactions involving only deuterons, protons, or neutrons as light particles, on a Li^7 target. The formulae of the simplest plane-wave theory involve the Fourier transforms of the bound-state wavefunctions corresponding to pairs of clusters whose trajectories are shown as double lines.

Textual references, pp. 55, 56.

FIGURE 15

IDENTIFICATION OF CLUSTERS IN DIRECT REACTIONS

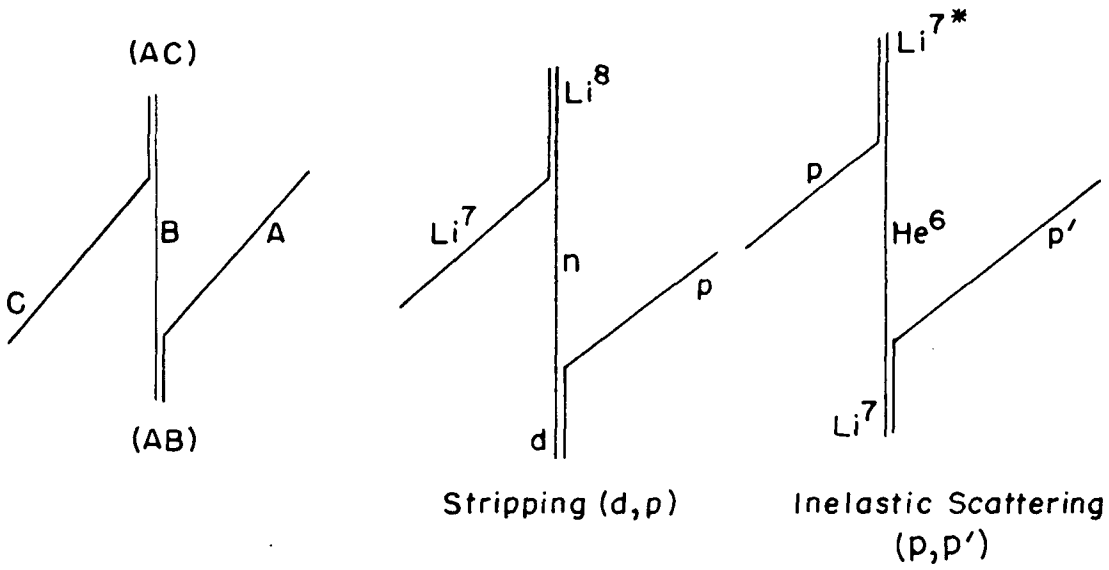

Stripping (d,p)

Inelastic Scattering (p,p′)

Knockout (p,n)

Pickup (p,d)

Heavy Stripping (d,p)

FIGURE 16

Vector Velocity Diagram for the Alpha Particles

This diagram illustrates the velocity vectors and the angles used in deducing the theoretical shape of particle spectra from a secondary breakup (Appendix A). The vector $\underset{\sim}{u}$ is the velocity of the center of mass of the over-all system relative to the laboratory, the vector $\underset{\sim}{v}$ is the velocity relative to the center of mass acquired in the first breakup, and the vector $\underset{\sim}{w}$ is the velocity acquired in the second breakup. The vector $\underset{\sim}{g}$ is the resultant velocity in the laboratory system, which makes an angle θ with the direction of the incident beam.

Textual references, pp. 65.

FIGURE 16

VECTOR VELOCITY DIAGRAM FOR THE ALPHA PARTICLES

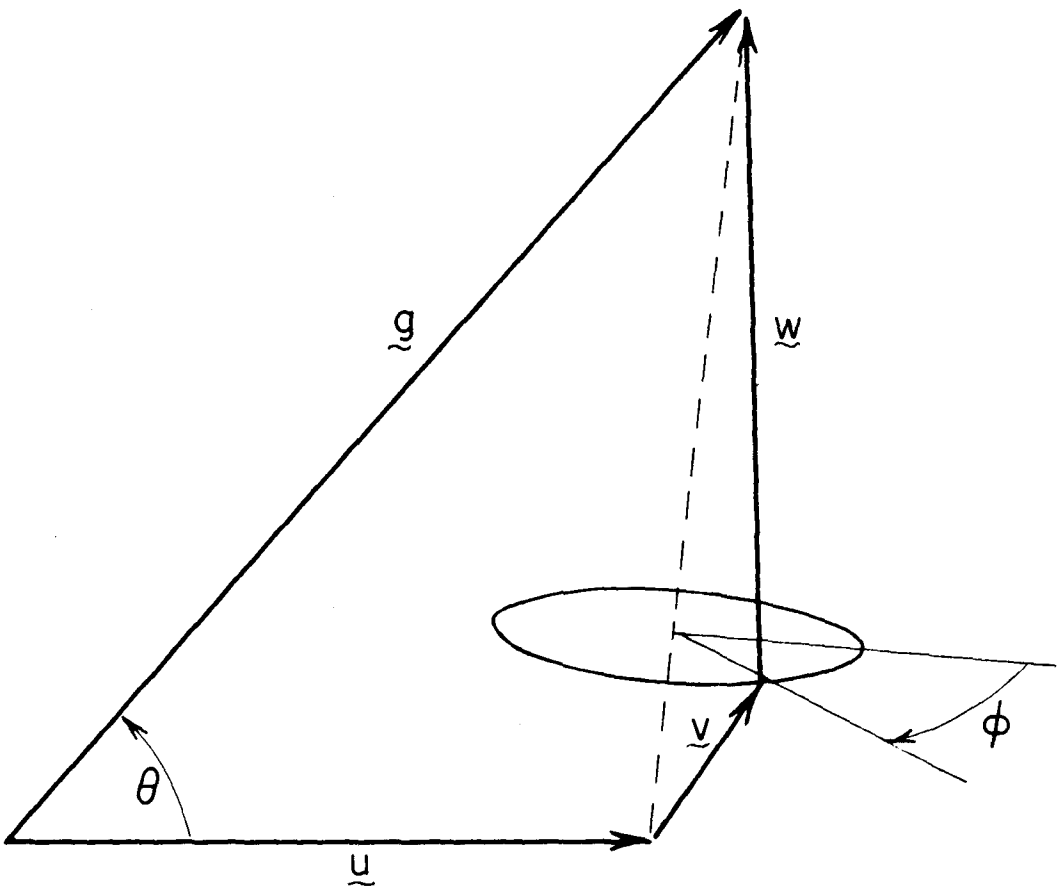

FIGURE 17

Nuclear Charge Density Assumed for the Deuteron Scattering

This is a graph of the nuclear charge distributions $\rho(r)$ assumed in the deduction of effective potentials to be used in calculations of the effect of the electrical polarizability of the deuteron on the elastic scattering (Appendix C). The dashed curve represents a uniform distribution, leading to the interaction (C.14). The solid curve represents the function $1/[(r/b)^6 + 1]^{3/2}$, which is the charge distribution which leads to an effective potential (C.15).

Textual references, pp. 89.

FIGURE 17

NUCLEAR CHARGE DENSITY ASSUMED FOR THE DEUTERON SCATTERING